SPATIALLY RESOLVING SPECTROMETER FOR CHARACTERISATION OF BROAD-AREA LASER DIODES

by

SHELDON VICTOR FERNANDES

Presented to the Faculty of the Graduate School of

The University of Texas at Arlington in Partial Fulfillment

of the Requirements

for the Degree of

MASTER OF SCIENCE IN ELECTRICAL ENGINEERING

THE UNIVERSITY OF TEXAS AT ARLINGTON

August 2007

ACKNOWLEDGEMENTS

I would like to express my utmost gratitude to my thesis advisor Dr. Nikolai Stelmakh for his guidance, encouragement & patience throughout this thesis. I thank him for allowing me to be a part of his research group. He has been a great mentor from whom I have learnt many aspects of research work.

I would like to thank Dr. J. C. Chiao & Dr. M. Vasilyev for accepting to be in my thesis supervisory committee.

I would also like to thank my friends Muthiah Annamalai for his technical advice & discussions on the thesis topic & Mr. K. K. Thomas for his suggestions in the layout of my thesis.

July 23, 2007

ABSTRACT

SPATIALLY RESOLVING SPECTROMETER FOR

CHARACTERISATION OF BROAD-AREA

LASER DIODES

Publication No. _____

Sheldon Victor Fernandes, M.S.

The University of Texas at Arlington, 2007

Supervising Professor: Dr. Nikolai Stelmakh

The mode pattern of the BALD (Broad-Area Laser Diode) is characterized and measured using a 1-GHz resolution double-pass spectrometer. The design of spectrometer allowed also a spatial discrimination with 1μm resolution. The construction and design of the double-pass grating is analyzed and discussed. A matrix approach is developed for the double-pass measurement arrangement. The developed procedure of analysis of spatially resolved spectra provides unique information about broad-area laser diode active medium and cavity geometry and potentially will help to predict the reliability of the laser diode. The developed model is based on paraxial approximation.

The laser diode modes are measured in the near-field & far-field. Measurements of spatially & spectrally resolved spectra of the laser radiation as a function of pumping current and observed polarization are conducted for laser diodes of different geometries.

Obtained data suggests that a careful choice between the length and width of BA laser diode cavity will help to avoid the coherence kink phenomenon and, therefore, will significantly improve the overall reliability of BALDs.

TABLE OF CONTENTS

LIST OF ILLUSTRATIONS

LIST OF TABLES

CHAPTER 1

INTRODUCTION

1.1 Motivation of this thesis

Spatially resolved spectroscopy of BALD cavity modes is the central point of the thesis. Using the double-pass grating spectrometer, the mode spectra in the near-field & far-field are displayed simultaneously side by side on the same output image.

Two aspects of the mode pattern structure of the BALD, which can be studied from this thesis work, are under consideration. Firstly, the efficiency of light delivery from the BALD, to the external devices, strongly depends on the distribution of the light energy between several lateral modes. A control of mode energy distribution is very important task to optimize the coupling efficiency. In a (BALD), a cavity structure whose output mode pattern allows maximum coupling efficiency of power transmission to other devices is desired.

The second aspect is in BALD reliability improvements. From the mode pattern of the BALD, its cavity structure & reliability can be analyzed. Some information about possible defect of the laser active medium can be recovered from the measured mode pattern.

1.2 Thesis Structure

This thesis is structured in the following manner.

In Chapter 2, a brief description of broad-area laser diodes is given. The cavity modes of the laser diodes are introduced. Using the rectangular cavity model, we find the wavelength separation & angular separation between the modes of the laser diode. The spectral & spatial distribution is related with the mode numbers.

In Chapter 3, the modes of the laser diode need to resolved & identified with a high accuracy. In order to develop an instrumentation system to do such a measurement, we need to find an arrangement to that will give a high resolution. The idea of the double-pass structure is analyzed. The setup of the double-pass grating spectrometer is shown. The various optical elements that make up the system are explained. The double-pass grating equation is derived.

In Chapter 4, the theory of matrix optics is introduced in Appendix A. The theory of the ray matrix of the diffraction grating is explained in Appendix B. A model of the double-pass grating system is derived & built up using the ray transfer matrix optics approach.

In Chapter 5, this section shows the procedure to measure the modes of the laser diode. The initial adjustments of the elements are explained. The procedure of performing the measurement & acquisition of the modes of the laser diodes using the computer is explained. The optical power measurement is also explained.

In Chapter 6, the output spectra for a BALD at various current values are shown.

In Chapter 7, various improvements that could be done on the double-pass spectrometer are suggested. These are mainly to streamline and automate the operation of this instrumentation system.

CHAPTER 2

MODES OF LASER DIODE

2.1 Introduction

A brief description of broad-area laser diodes is given. The cavity modes of the laser diodes are introduced. Using the rectangular cavity model, we find the wavelength separation & angular separation between the modes of the laser diode. The spectral & spatial distribution is related with the mode numbers.

2.2 Broad-area laser diodes

Broad-area laser diodes (BALDs) are edge-emitting devices [5] where the emitting region (the active medium) at the front facet has the shape of a broad line i.e. the width of the laser diode active medium is much larger in dimensions compared with its height. It is in this emitting region that the injection current is confined & the recombination of carriers takes place. Typically a laser diode emitter width is normally in the range of 50μm - 200μm and length in the order of 1-5 mm. A BALD is normally used in applications that require high power.

The geometry of high-power laser diodes varies from single ~10 μm narrow stripe emitting several hundred milliwatts to 100-200μm wide broad-area lasers emitting a few watts. Also there are more complex geometries involving multiple diode lasers such as laser diode bars and matrices emitting several watts.

For single element emitter, the simplest way to increase the emitted power is to increase the size of the emitting aperture, but the beam quality is adversely affected. Instead of Gaussian distribution (single mode) of amplitude and uniform phase distribution across the whole facet, the output of a broad area device is usually divided into many incoherent regions (multi-mode) which don't have a constant phase relationship. The laser output therefore becomes a sum of individual intensities of these incoherent regions, and loses its diffraction limited virtue. This is illustrated in Fig. 2.1 below. The yellow emitter region is the active medium which is sandwiched between the p & n regions.

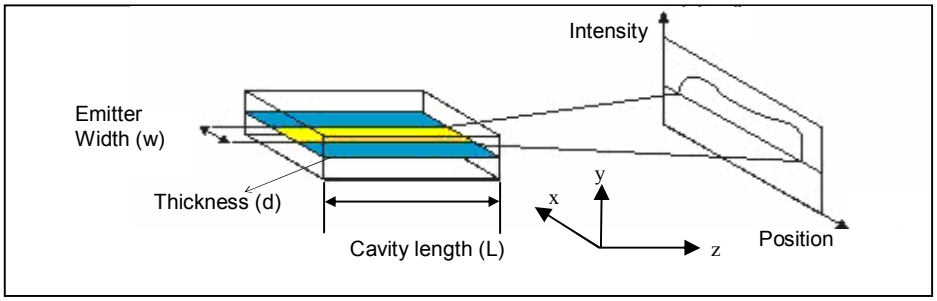

Figure 2.1: Illustration of a typical BALD device & its intensity profile as a function of position along the emitter. [6]

2.3 Cavity modes of a laser diode

A waveguide mode is an electromagnetic wave that propagates along a waveguide with well-defined characteristics like phase velocity, group velocity, cross-sectional intensity distribution, and polarization [2.4]. These characteristics depend on the shape & composition of the waveguide. The modes are referred to as "characteristic waves" of the waveguide because their field vectors satisfy the homogeneous wave

equation in all the media that make up the guide, as well as the boundary conditions at the interfaces.

In the laser diode, the active medium is in the form of a rectangular cavity. This region acts as a waveguide to the laser radiation generated within the medium. The structure and composition of this waveguide cavity determines the characteristics of the laser radiation emitted by the laser diode and hence the nature of the modes.

Typically the cavity is in the form of a Fabry-Perot cavity. Now, because the index of the active region varies with the wavelength, the longitudinal modes produced due to the Fabry-Perot cavity are not equally spaced. As seen in Fig 2.1, the cavity length L determines the modal spacing between the longitudinal modes. The emitter width w determines the transverse modes that are produced. The height d along with the cavity structure determines the optical confinement factor & is constructed such that only the fundamental mode exists [2.2].

The output spectra of the laser diode consist of groups of transverse modes separated by the longitudinal mode period.

2.3.1. Longitudinal mode separation

The mode frequency is given by

$$f_m = m\frac{c}{2n_{ph}(\lambda)L\cos\theta} \tag{0.1}$$

where m is the mode number, c is the velocity of light in free space, $n_{ph}(\lambda)$ is the phase index of refraction in the active medium. L is the cavity length & θ is the angle between the two ends of the cavity [2.1]. (For parallel ended cavity we have $\theta = 0$)

The frequency separation between two consecutive mode frequencies is given by

$$\Delta f_m = \frac{c}{2n_{ph}(\lambda_0)L} \tag{0.2}$$

Expressing (0.2) in terms of wavelength difference, we have

$$\frac{1}{\Delta\lambda} = \frac{1}{2n_{ph}(\lambda_0)L} \tag{0.3}$$

The wavenumber N is defined as

$$N = \frac{n_{ph}(\lambda_0)}{\lambda} \tag{0.4}$$

If ΔN is the difference in wave number between two adjacent longitudinal modes, then from (0.3) & (0.4)

$$\Delta N = \frac{1}{2L} \tag{0.5}$$

But since the active medium is dispersive, the relation between N & λ is obtained from (0.4)

$$\frac{dN}{d\lambda} = \frac{1}{\lambda}\frac{dn_{ph}(\lambda_0)}{d\lambda} - \frac{n_{ph}(\lambda_0)}{\lambda^2} \tag{0.6}$$

Rearranging (0.6) & substituting (0.5)

$$\Delta\lambda = \frac{\lambda^2}{2n^*(\lambda_0)L} \tag{0.7}$$

where $n^*(\lambda_0) = n_{ph}(\lambda_0) - \lambda \frac{dn_{ph}(\lambda_0)}{d\lambda}$ is the group index of refraction of the active medium.

Typical longitudinal mode separation for a laser diode is around 1.256 Angstrom [3.1]

As seen from (0.7) the longitudinal mode separation depends on the cavity length, the refractive index & the dispersion in the active medium.

2.4 Standing wave condition inside the BALD cavity

Consider a laser cavity in the form of a two-dimensional dielectric slab waveguide. The graphical representation of slab is shown in Fig. 2.2. The *L* is the laser cavity length, *w* is the stripe width, $n(\lambda_0)$ is the phase refraction index at wavelength λ .

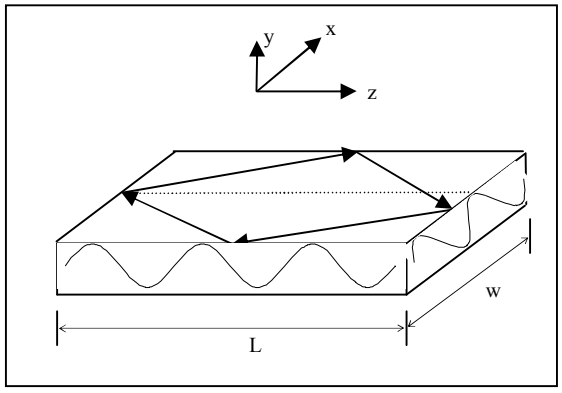

Figure 2.2: Laser Diode as a Fabry-Perot cavity which forms standing wave modes.

To satisfy the standing wave condition in the *z*-direction, an integral number of half-wavelengths must exist through the length *L*. Here *m* is referred to as the mode number.

$$m\frac{\lambda}{2} = L \qquad (0.8)$$

Rewriting (0.8) we have

$$\frac{m}{L}=\frac{2}{\lambda}$$
$$\frac{\pi m}{L}=\frac{2\pi}{\lambda} \tag{0.9}$$

Therefore the wave vector component in the z-direction can have only discrete values multiple of m

$$\vec{k}_z=\frac{\pi m}{L} \tag{0.10}$$

Similarly in the x-direction we have,

$$p\frac{\lambda}{2}=w \tag{0.11}$$

Rewriting (0.11) we have

$$\frac{p}{w}=\frac{2}{\lambda}$$
$$\frac{\pi p}{w}=\frac{2\pi}{\lambda} \tag{0.12}$$

Therefore the wave vector component in the x-direction is

$$\vec{k}_x=\frac{\pi p}{w} \tag{0.13}$$

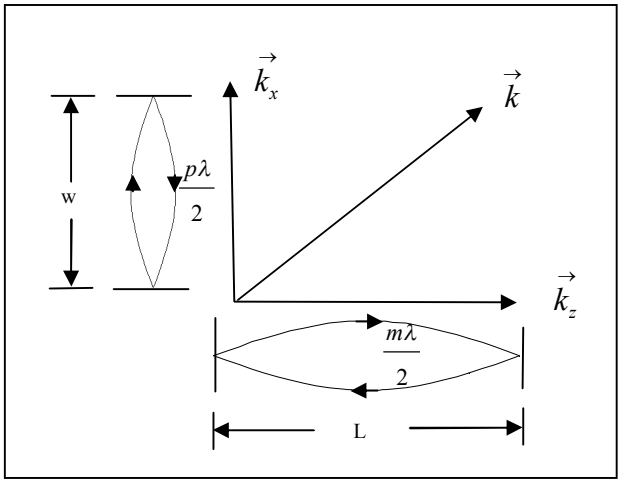

Figure 2.3: k Wave-vector & the standing wave condition

The $\vec{k}$ vector of the 2D cavity is given by

$$\vec{k}^2 = \vec{k}_z^2 + \vec{k}_z^2 \tag{0.14}$$

This is illustrated in Fig 2.3 where the wave vector $\vec{k}$ of the cavity is given by

$$\vec{k} = \frac{2\pi}{\lambda_0} n(\lambda_0) \tag{0.15}$$

Substituting (0.10), (0.13) and (0.15) into (0.14) we get,

$$\left(\frac{2\pi n(\lambda_0)}{\lambda}\right)^2 = \left(\frac{\pi m}{L}\right)^2 + \left(\frac{\pi p}{w}\right)^2 \tag{0.16}$$

$$\frac{4n(\lambda_0)^2}{\lambda^2} = \frac{m^2}{L^2} + \frac{p^2}{w^2} \tag{0.17}$$

$$\lambda = \frac{2n(\lambda_0)}{\sqrt{\frac{m^2}{L^2} + \frac{p^2}{w^2}}} \tag{0.18}$$

Since *p/w << m/d* for a BALD, the above equation can be written as

$$\lambda_{m,p} = \frac{2n(\lambda_0)}{\frac{m}{L}\sqrt{1+\left(\frac{pL}{wm}\right)^2}} \tag{0.19}$$

Using Taylor Series, we can express the above equation as

$$\lambda_{m,p} = \frac{2n(\lambda_0)L}{m} \cdot \left(1 - \frac{1}{2}\left(\frac{pL}{wm}\right)^2\right) \tag{0.20}$$

2.5 Mode pattern of the spectra in the far-field

Consider a laser cavity in the form of a two-dimensional As seen from (0.20), the spectral position of the modes is determined by *m* & *p*. For a particular mode group *m* we can calculate the spectral position of a particular mode *p*.

Once the modes are resolved, they are distributed spatially distributed in the far-field. For a particular longitudinal mode group number *m*, the transverse mode numbers *p* are spread angularly across the far-field. This is shown in Fig 2.3. The near-field spectra on the left & far-field spectra on the right are shown for a BALD. In the far-field spectra, the variation of the modes of mode number *p* both spectrally in terms of wavelength & spatially in terms of its angular position across the space is observed. The variation of the mode pattern is parabolic in nature. This particular pattern of distribution of the intensities can be explained as follows.

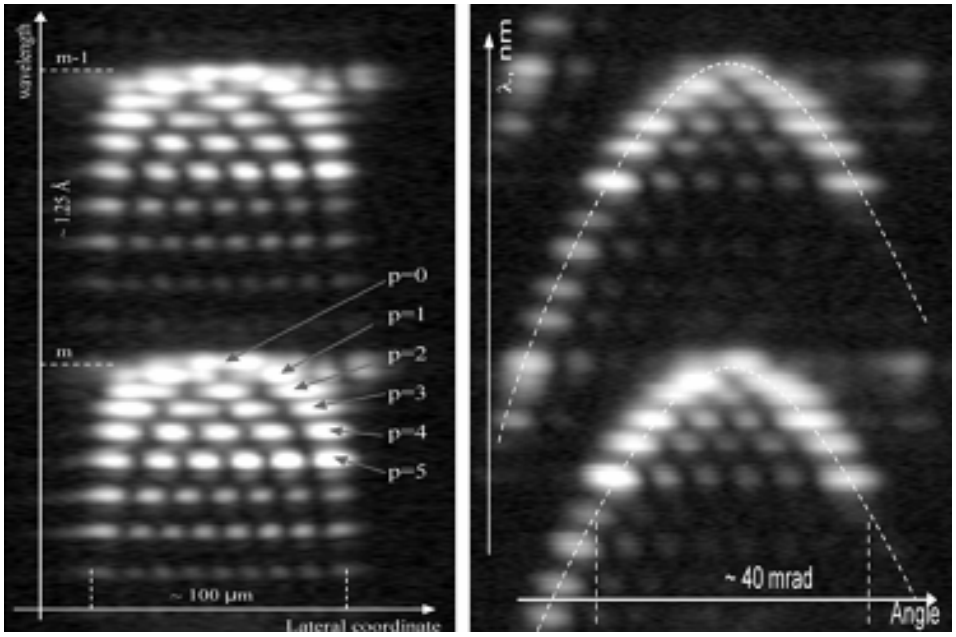

Figure 2.4: Near-field (left image) & far-field (right image) intensity spectra of two longitudinal mode intervals. For illustration purpose the intensity axis is logarithmic [3.1]

The angular separation between the modes of a particular mode number p is given by [3.2]

$$\Delta\theta_p = \frac{2\lambda_0}{w}\sqrt{p^2 - 1} \tag{0.21}$$

From (0.19), we can calculate the spectral position of the modes, for mode number *p* from 1 to 5. This is shown in Fig 2.4.

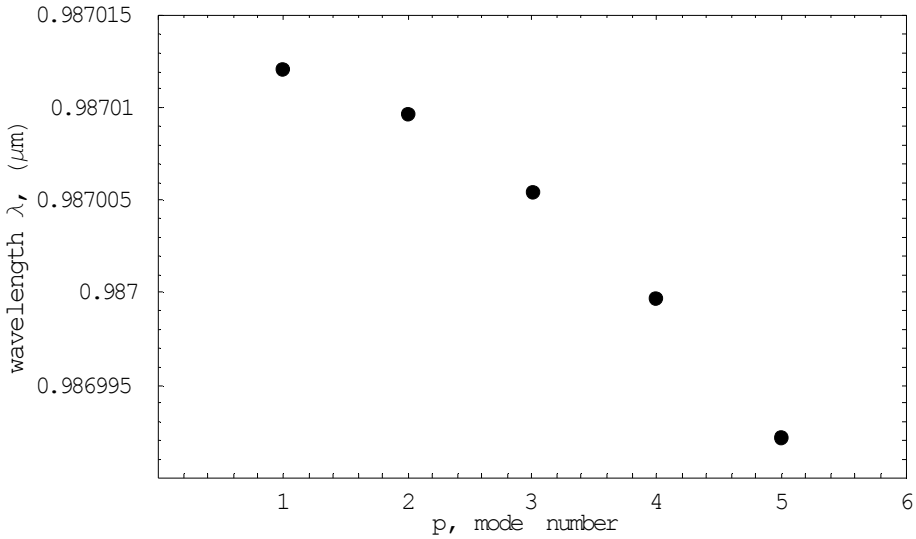

Figure 2.5: Spectral positions of modes as a function of mode number p. Data plotted for longitudinal mode number m=7700, phase index of refraction of the active medium $n(\lambda_0)$ = 3.8, cavity length L=1000μm, stripe width w=100 μm

Using (0.21) we can calculate the angular separation between the intensity peaks for each mode number p. This is shown in Fig 2.5.

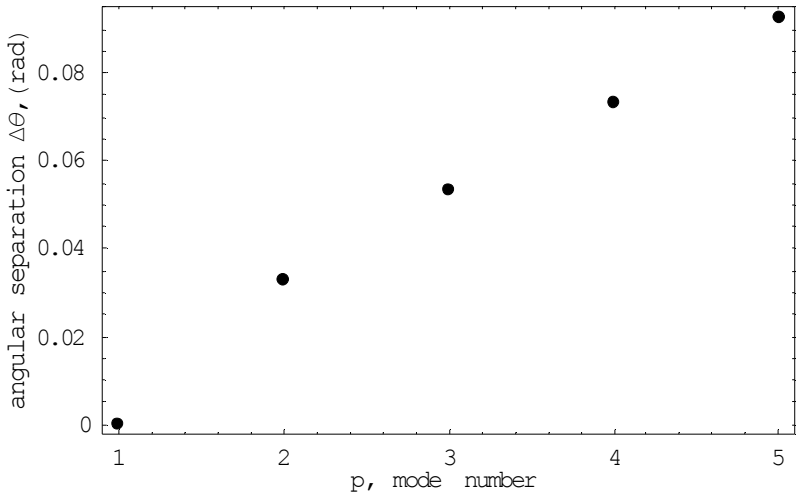

Figure 2.6: Angular separation between modes as a function of mode number p. Data plotted for longitudinal mode number λ_0 =0.95 μm, phase index of refraction of the active medium $n(\lambda_0)$ = 3.8, cavity length L=1000μm, stripe width w=100 μm

By combining the graphs Fig 2.5 & Fig 2.6, we can find the spatial position of the spectrally resolved modes for each of the mode numbers *p*. This is shown in Fig 2.7

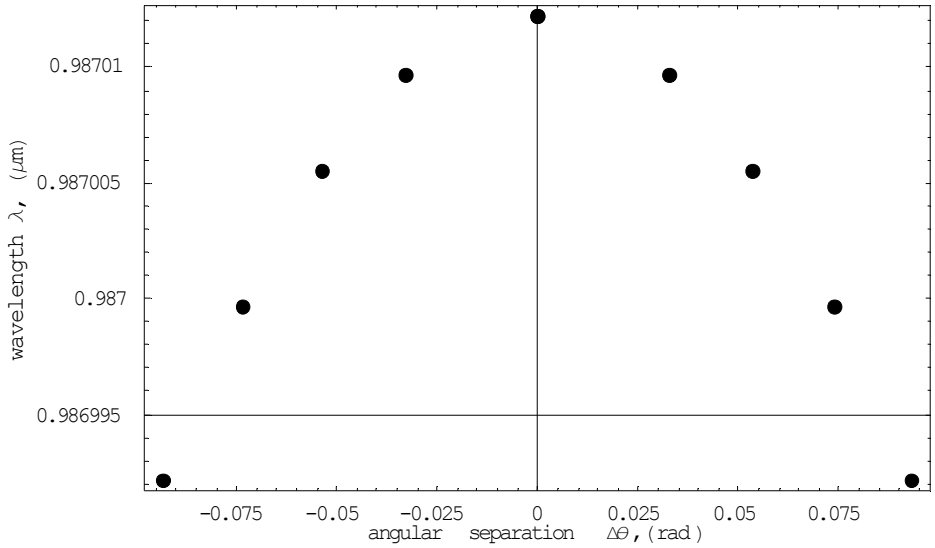

Figure 2.7: The spatial distribution of the spectrally resolved modes in the far-field. The position of the peaks in the far-field corresponding to the observed intensity spectra in Fig: 2.4. The mode number keeps increasing from top to bottom of the graph.

The wavelength separation between two modes for a BALD described in Fig 2.4 can be calculated using (0.20) and is of the order of 0.025 Angstrom.

To resolve and identify each mode in the output spectra we need an instrumentation system that is capable of resolving modes spectrally in the order of Angstroms.

CHAPTER 3

DOUBLE-PASS SPECTROMETER SYSTEM

3.1 Introduction

The modes of the laser diode need to resolved & identified with a high accuracy. In order to develop an instrumentation system to do such a measurement, an arrangement is needed that will give a high resolution. The idea of the double-pass structure is analyzed. The setup of the double-pass grating spectrometer is shown. The various optical elements that make up the system are explained. The double-pass grating equation is derived.

3.2 Principle of the Double-pass spectrometer

To study & observe the mode structure of the laser diode, a diffraction grating is used to resolve the modes of the laser diode. The beam is spatially resolved in the lateral direction. Since high-resolution is preferred to resolve & distinguish each mode of the laser diode, a double-pass approach of the grating is used. The idea is that if the beam is passed through the grating twice, the effective number of grooves is doubled & hence the resolution is also doubled according to the Rayleigh criterion [3.1]. The laser beam is passed twice into the grating using a mirror to reflect the beam back to the grating the second time. According to the Rayleigh criterion, we have the optical diffraction limit between two wavelengths given by

$$\Delta\lambda = \frac{\lambda_0}{N} \tag{3.1}$$

λ_0 is the central wavelength of the beam & N is the effective number of grooves.

The effective number of grooves for a grating of length L_{groove} = 50mm & a grooves/mm as n_{groove} = 2000 is given by

$$N = n_{grooves} * L_{groove} \tag{3.2}$$

Thus N is given by 10000. For a double-pass configuration, the effective number of grooves is doubled. Thus we have N = 2*10000 = 20000 grooves. For a wavelength of 970 nm, we have the theoretical resolution given by

$$\Delta\lambda = \frac{\lambda_0}{N} = \frac{970*10^{-9}}{2*10^5} = 0.00485nm \tag{3.3}$$

This corresponds to a frequency resolution of

$$\Delta f = \frac{c}{\lambda_0} - \frac{c}{(\lambda_0 + \Delta\lambda)} = 1.546GHz \tag{3.4}$$

Due to high signal-to-noise ratio of the acquired images, the resolution limit in resulting images is about 1GHz.

After the double-pass, an optical setup is used to project the near-field & far-field output of the resolved beam simultaneously onto the camera. This enables us to compare the near-field & far-field on the same output image. The entire setup is controlled using a computer. The rotation of the grating & the capture of the output images are done in an automated manner through a computer.

3.3 System Setup of the double-pass grating spectrometer

The system setup is shown & the block diagrams of the various optical elements are illustrated. The path of the laser beam is shown as it passes through the setup.

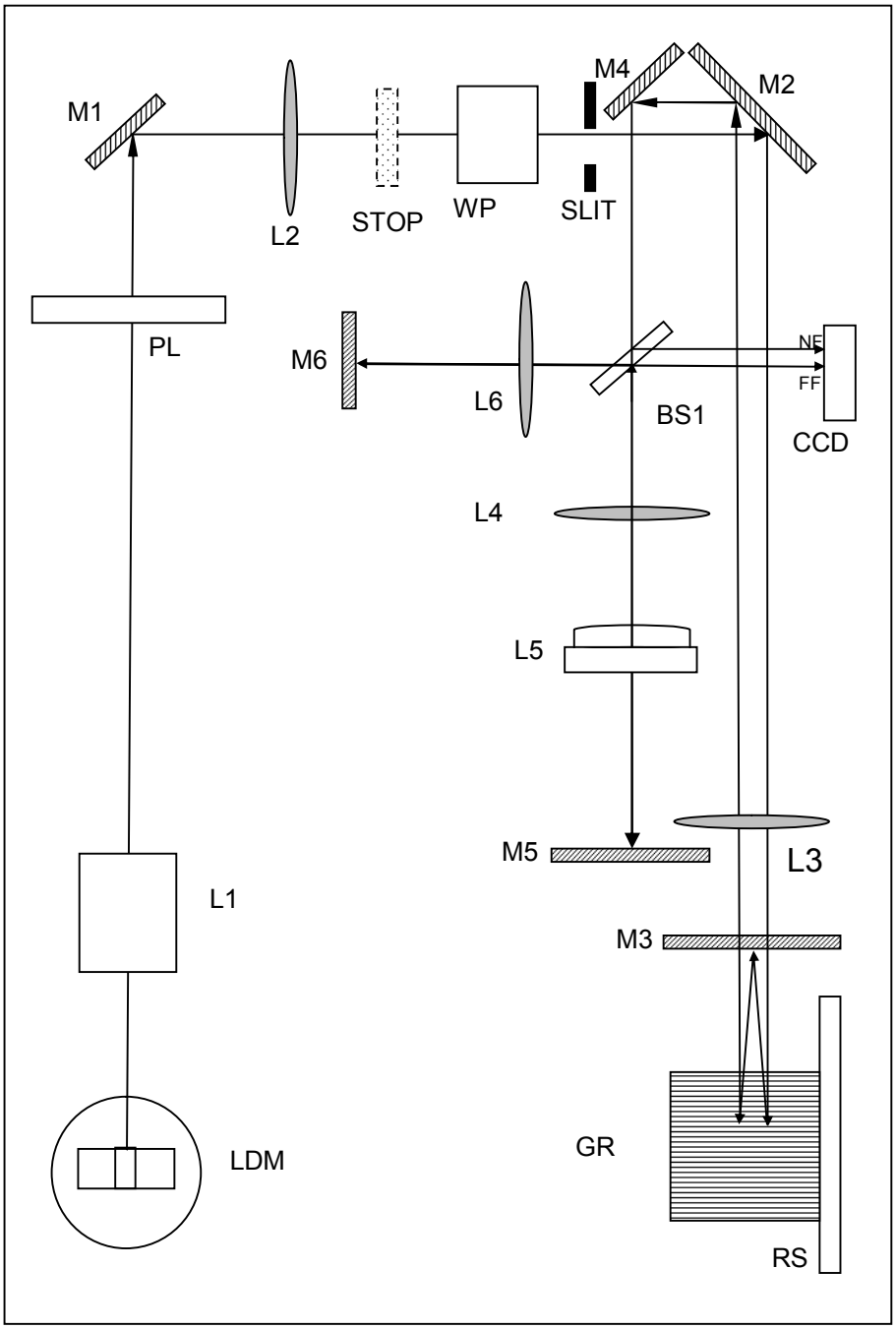

Figure 3.1: System level diagram of the double-pass grating spectrometer setup.

The overview of the double-pass grating along with the various optical elements & the path of the beam are shown in Fig 3.1.

3.3.1 Photograph of the double-pass grating system with the light path.

Fig 3.2 shows the photograph of the double-pass grating spectrometer system. The laser beam path through the system is color coded for easier identification. The entire setup is on an optical table and in room temperature conditions.

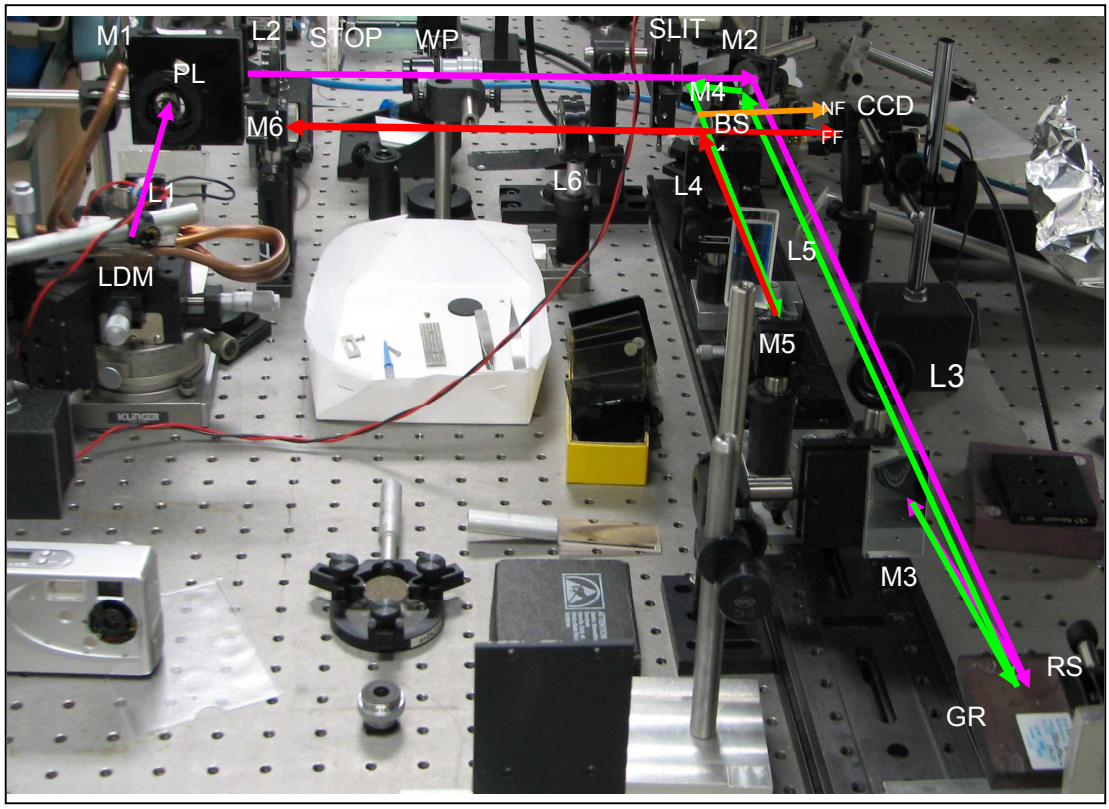

Figure 3.2: Photograph of the system showing the path of light rays entering and exiting the system.

3.4 Double-pass grating system elements

The various elements of the double-pass spectrometer are shown & explained. The path of the laser beam through the various elements is shown to give more clarity

3.4.1 Laser diode mount LDM

The laser diode mount consists of water cooled mount where the laser diode can be securely placed. The mount is then placed on a translation stage with adjustments in three dimensions & angular adjustments as shown in Fig 3.3

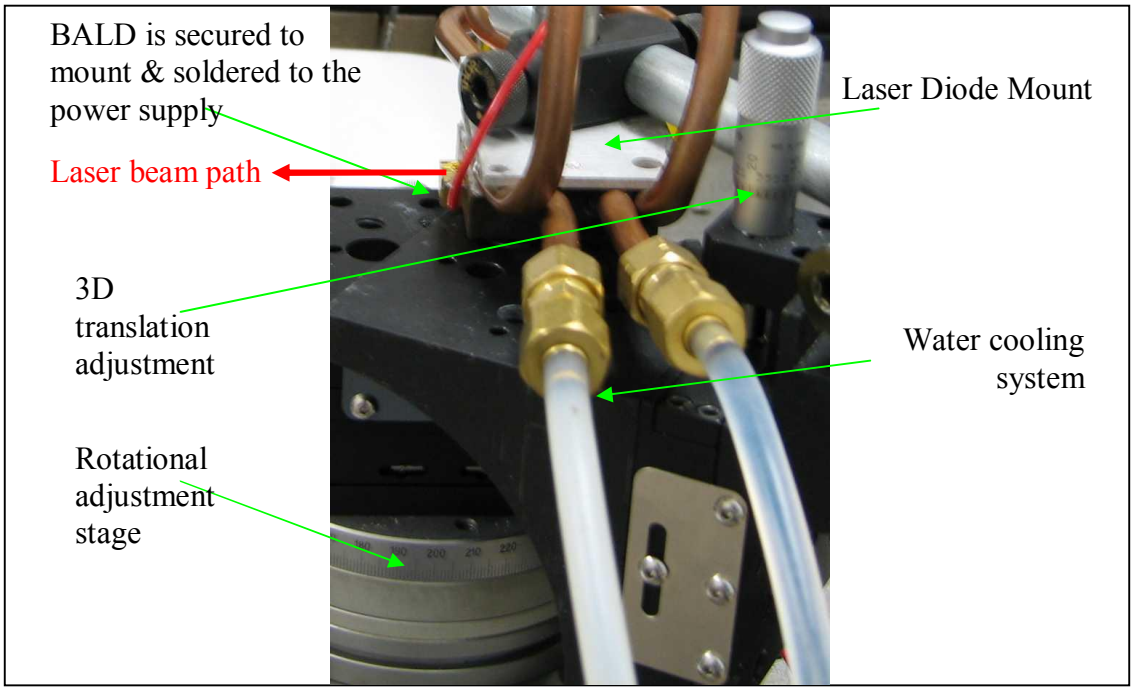

Figure 3.3: Water cooled laser diode mount system attached to translation stage.

3.4.2 Lenses L1 & L2 & Input slit SLIT

Lenses L1 & L2 are used to collimate & focus the beam so that it is properly focused when it passes through the slit. The input slit is used to prevent back reflection & limit the power carried by the beam. The lenses L1 & L2 are positioned in such a

way that distance from the laser to L2 is equal to the distance from L2 to the SLIT and is the focal length of the lens L2. The input slit is used to prevent back reflection & limit the power carried by the beam.

3.4.3 Polarizer PL & half waveplate WP

The polarizer PL is used to linearly polarize the laser beam in the orientation of maximum intensity. After the beam is linearly polarized, it is passed through a half-waveplate WP to make adjustments to the orientation of the beam.

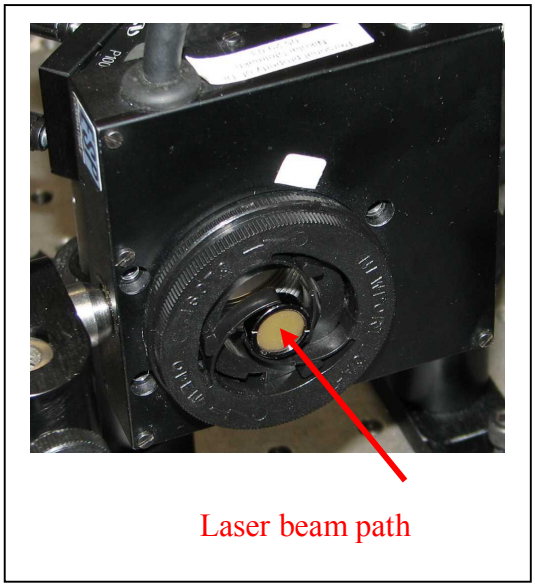

Figure 3.4: Polarizer (PL) is used to make the beam linearly polarized to get maximum intensity & this can be rotated using a motor controlled by the computer.

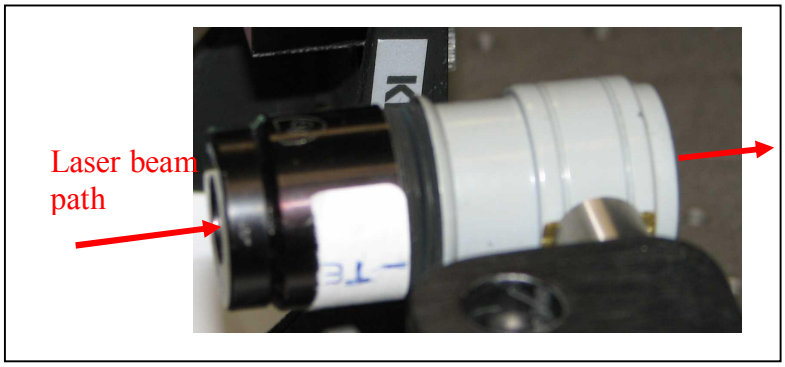

Figure 3.5: Half waveplate (WP) used to adjust the orientation of the linearly polarized beam.

Putting all these elements together we have the following arrangement as shown in Fig 3.6

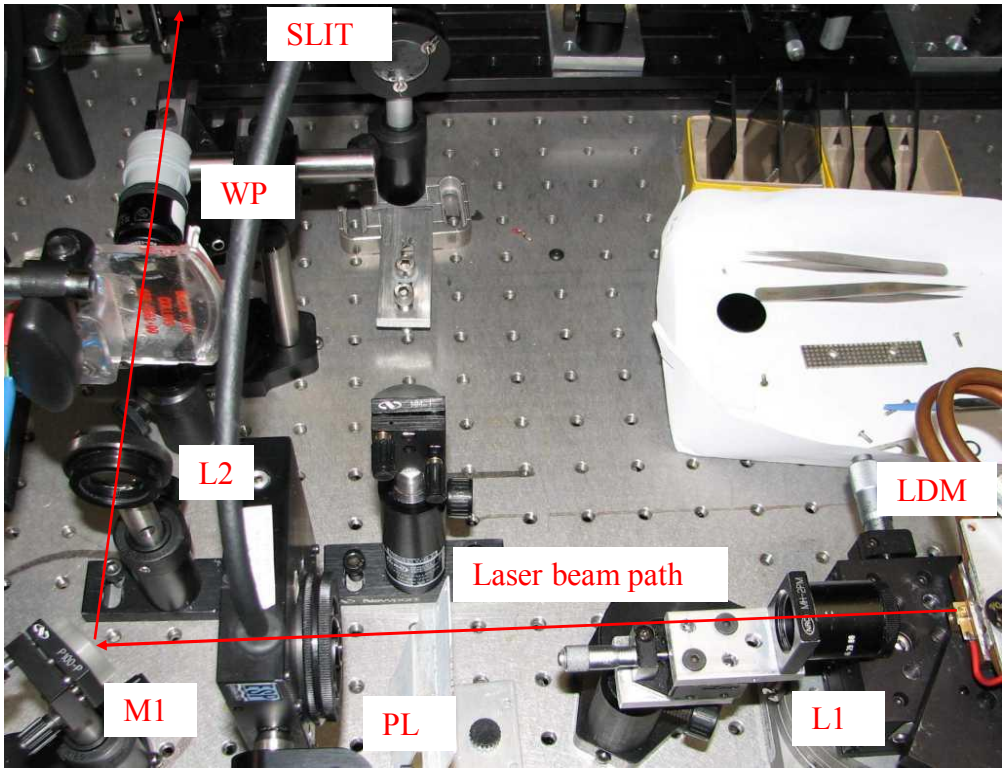

Figure 3.6: To maintain the focus of the beam, distance from LDM to L2 is equal to distance from L2 to slit and is the focal length of lens L2

3.4.4 The double-pass grating arrangement

This consists of the collimating lens L3, the rotating stage RS, the grating GR & the double pass mirror M3. The lens L3 is positioned in such a way that distance from SLIT to L3 is equal to distance from L3 through GR, M3 and back to L3 and is the focal length of lens L3.

The beam passes through L3 when entering the grating system & leaving it. From L3 the beam passes into the NFFOS [3.1]. To ensure that the beam is in focus, the distance from L3 to the beam-splitter is equal to the focal length of lens L3.

The rotating stage RS is holds the grating and is controlled using a controller, it is also controlled using the computer through software. The grating GR has a groove density of 2000 per mm. The input beam is aligned at the center of rotation of the grating. The mirror M3 is aligned at the double-pass position to the input beam with respect to the grating. The distance between the grating and the mirror is fine tuned during calibration. This arrangement is shown in Fig 3.7

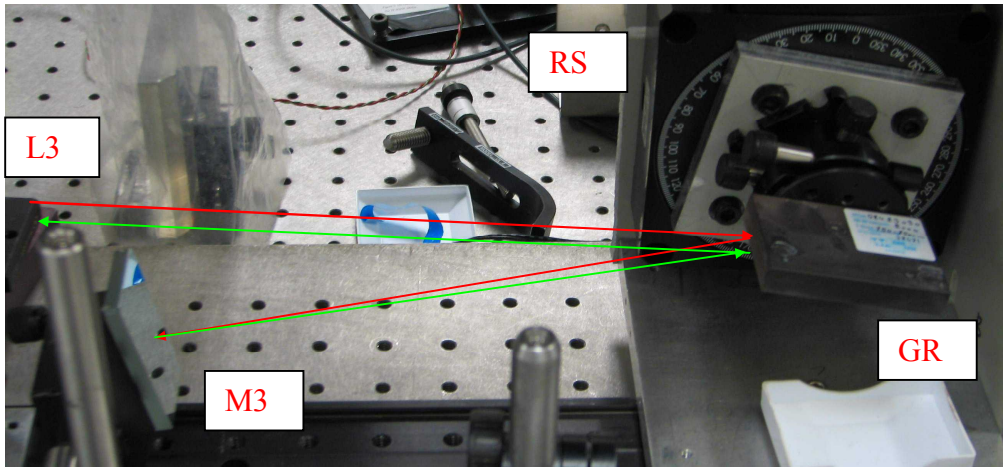

Figure 3.7: To maintain the focus of the beam, distance from SLIT to L3 is equal to distance from L3 through GR, M3 and back to L3 and is the focal length of lens L3

3.4.5 The NFFFOS (Near-Field Far-Field Optical Setup)

This consists of a beam-splitter BS1, which splits the beam into two components. One component forms the near-field spectra of the output beam & the other component goes in the NFFFOS where it is transformed into the far-field spectra.

Lenses L4 & L6 are collimating lens while L5 is the cylindrical lens [3.1]. This is illustrated in Fig 3.8

The optical system has total spatial dispersion of 2.0 μm/pixel and horizontal angular (in far-field measurement area) dispersion of 4.0 mrad/pixel [3.1].

During the acquisition of the spectrum, the linear CCD Si camera captures images for several angular positions of the grating. The images are then resampled and stitched together using the dispersion formula of the spectrometer.

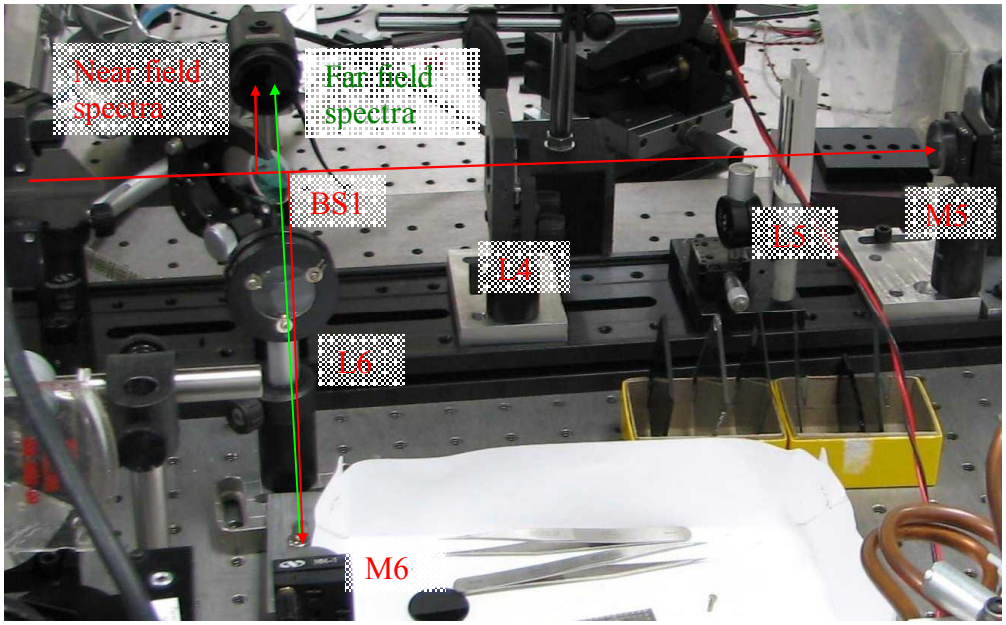

Figure 3.8: The NFFFOS is used to transform the resolved beam to get the far-field. L4 & L6 act as the collimating lenses. L5 is the cylindrical lens.

3.4.6 Support Equipment

The support equipment for the double-pass grating spectrometer consists of the laser diode power supply, the rotating stage controller, the output TV monitor, the power meter.

Figure 3.9: Double-pass grating system support equipment includes LD power supply, a TV monitor, rotation stage controller and a power meter.

3.4.7 Computer software

The experiment is performed and controlled using LabVIEW software. This includes the calibration, control, acquisition, image processing and output data.

Several VI modules are developed to perform different parts of the experiment.

3.5 Double-pass grating equation

The side view of the double-pass grating system is shown below, the relation between the input angle and the output angle is derived.

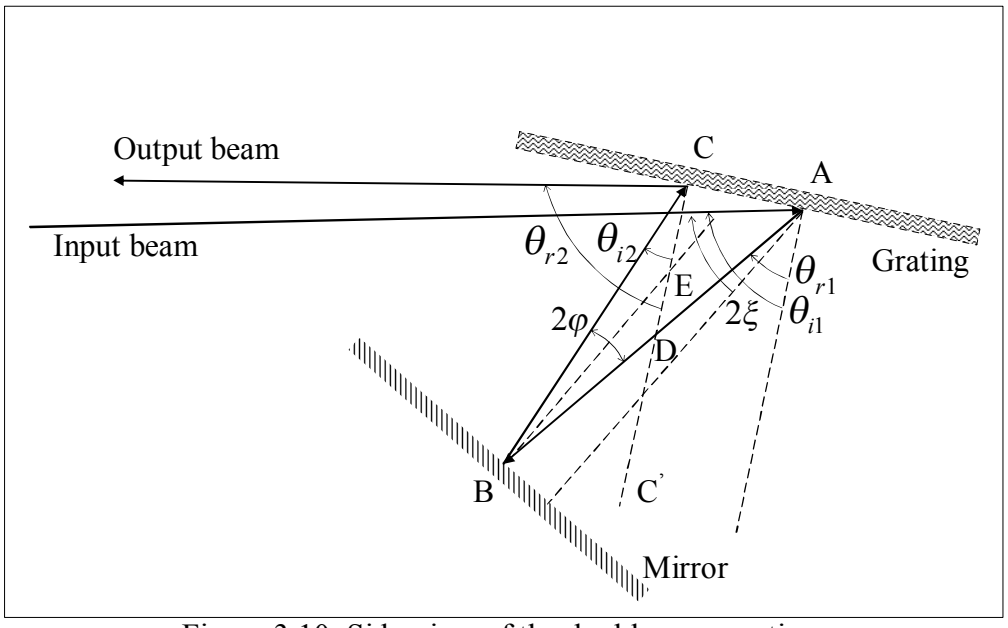

Figure 3.10: Side-view of the double-pass grating.

From Figure 3.10, at point A, the input beam falls on the grating with angle θ_{i1} w.r.t the grating normal. The diffracted beam has angle θ_{r1} w.r.t the grating normal.

$$\sin\theta_{i1} + \sin\theta_{r1} = \frac{\lambda_0}{d} \tag{3.5}$$

where λ_0 is the center wavelength & d is the groove distance.

At point C, the input beam falls on the grating with angle θ_{i2} w.r.t the grating normal. The diffracted beam has angle θ_{r2} w.r.t the grating normal.

$$\sin\theta_{i2} + \sin\theta_{r2} = \frac{\lambda_0}{d} \tag{3.6}$$

The mirror is placed with its normal at an angle 2ξ w.r.t the input beam. ξ is the half inclination angle of the double-pass mirror. It is the angle of the grating

corresponding to the back reflection from the double-pass mirror. i.e. the input angle & the output angle are the same.

$$2\xi = \theta_{i1} - \theta_{r1} + \varphi \tag{3.7}$$

In ΔBCD,

$$\begin{aligned} 2\varphi + \theta_{i2} + (\pi - \theta_{r1}) &= \pi \\ 2\varphi &= \theta_{r1} - \theta_{i2} \end{aligned} \tag{3.8}$$

Expressing equation in terms of φ & substituting in equation we get

$$\begin{aligned} \varphi &= 2\xi - \theta_{i1} + \theta_{r1} \\ 2(2\xi - \theta_{i1} + \theta_{r1}) &= \theta_{r1} - \theta_{i2} \\ \theta_{r1} + \theta_{i2} &= 2(\theta_{i1} - 2\xi) \end{aligned} \tag{3.9}$$

Expressing θ_{r1} in terms of θ_{i1} & θ_{i2} in terms of θ_{r2} using equations,

$$\sin^{-1}\left(\frac{\lambda_0}{d} - \sin\theta_{i1}\right) + \sin^{-1}\left(\frac{\lambda_0}{d} - \sin\theta_{r2}\right) = 2(\theta_{i1} - 2\xi) \tag{3.10}$$

The above equation is the double-pass grating equation which connects the input beam angle & the output beam angle.

If γ is the rotational angle of the grating in the plane parallel to the grating grooves. The double-pass grating equation can be rewritten as [3.1]

$$\sin^{-1}\left(\frac{\lambda_0 \cos\gamma}{d} - \sin\theta_{i1}\right) + \sin^{-1}\left(\frac{\lambda_0 \cos\gamma}{d} - \sin\theta_{r2}\right) = 2(\theta_{i1} - 2\xi) \tag{3.11}$$

γ varies for different lateral spatial components of laser emission.

Rewriting the above equation we get,

$$\sin^{-1}\left(\frac{\lambda_0 \cos\gamma}{d} - \sin\alpha_{in}\right) + \sin^{-1}\left(\frac{\lambda_0 \cos\gamma}{d} - \sin\alpha_{out}\right) = 2(\alpha_{in} - 2\xi) \tag{3.12}$$

Rearranging (3.12) we get,

$$\alpha_{out} = \sin^{-1}\left(\frac{\lambda_0 \cos\gamma}{d} - \sin\left(2\left(\alpha_{in} - 2\xi\right) - \sin^{-1}\left(\frac{\lambda_0 \cos\gamma}{d} - \sin\alpha_{in}\right)\right)\right) \qquad (3.13)$$

Using the above equation we can see the behavior of the grating system for different parameters as shown in the figures below. Figure 3.11 shows the variation of the output angle of the system with respect to the variation of the input angle.

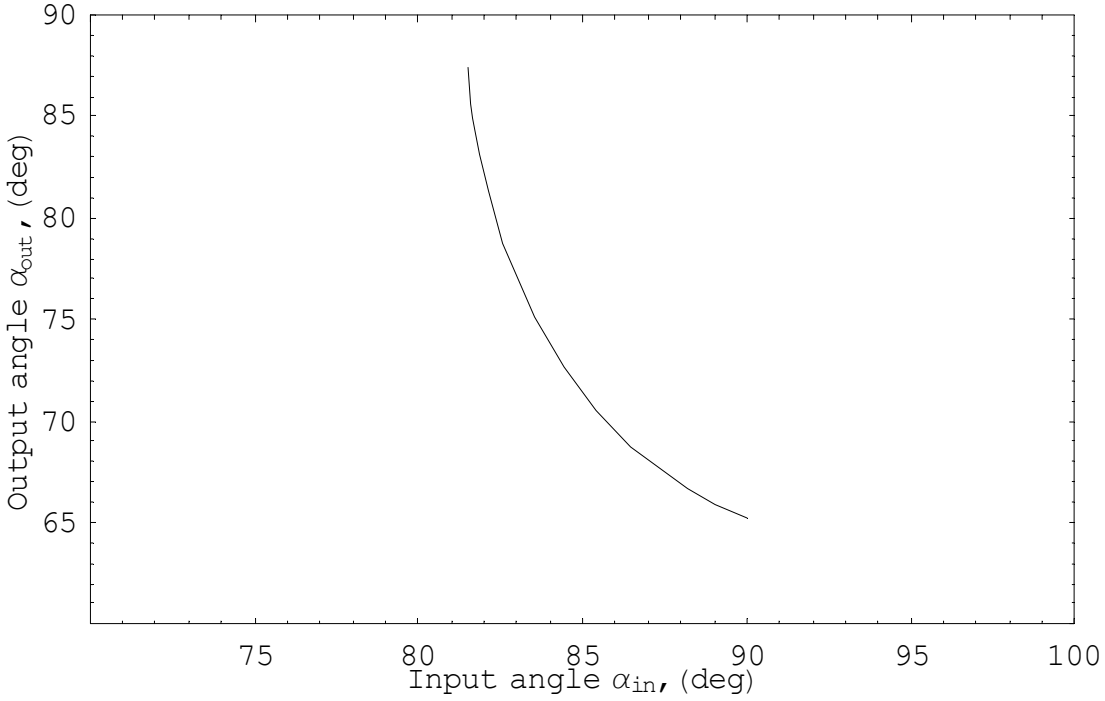

Figure 3.11: The variation of the double-pass grating input angle with output angle for λ_0=950nm, d=500nm & 2ξ=16.5 deg.

Figure 3.12 shows the variation of the output angle of the system with respect to the variation of the wavelength of light incident on the grating.

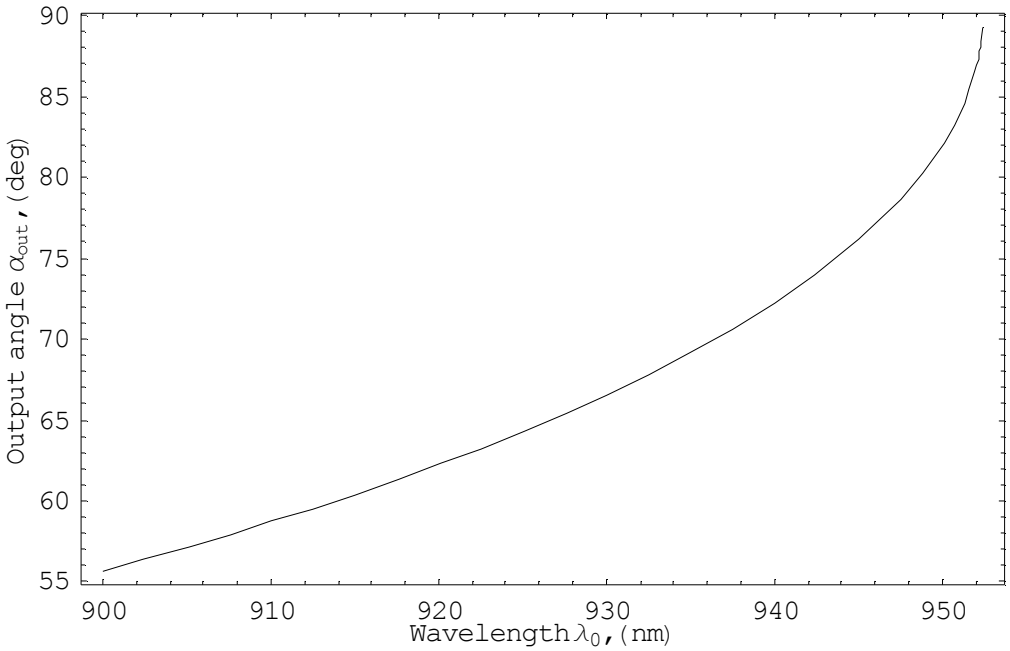

Figure 3.12: The variation of the double-pass grating output angle with wavelength of the beam for α_{in}=82 deg, d=500nm & 2ξ=16.5 deg.

CHAPTER 4

RAY TRANSFER MATRIX MODEL OF DOUBLE-PASS GRATING

4.1 Introduction

The theory of matrix optics is introduced in Appendix A. The theory of the ray matrix of the diffraction grating is explained in Appendix B. A model of the double-pass grating system is derived & built up using the ray transfer matrix optics approach.

4.2 Modeling the double-pass grating system

The ray matrix approach allows us to divide the double-pass grating system into components & the ray matrix section for each section is developed & all the sections are put together to make an entire model of the system.

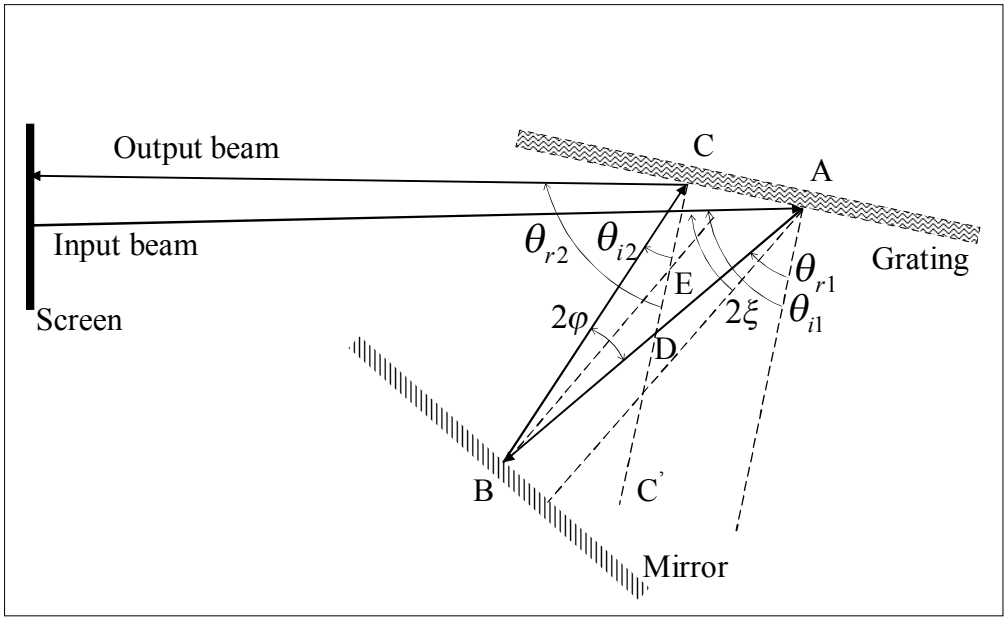

Figure 4.1: Comparison of the input beam & output beam from the double-pass grating

4.2.1 Sectioning of the double-pass grating system

Each optical ray path propagating through free space is considered as a section. Each optical element is considered as a section. Each of these sections is constructed using the 3X3 matrix approach.

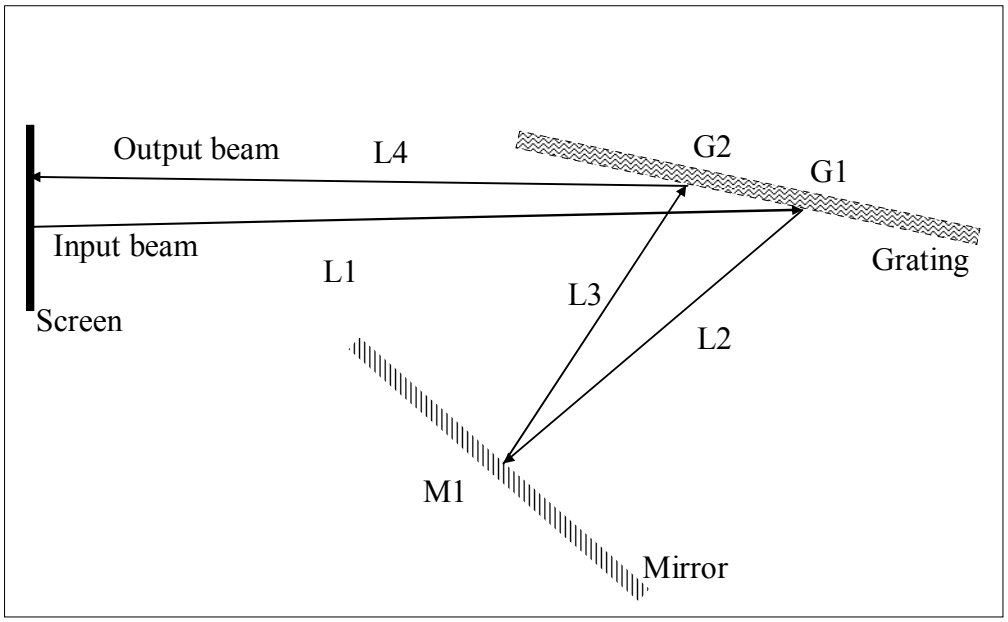

Figure 4.2: Section-wise diagram of the double-pass grating.

From the above figure, the optical path taken by the beam is through sections: L1, G1, L2, M1, L3, G2 and L4. The ray transfer matrix will be built up for each section and final. Let the screen be placed at the position of the collimating lens. The screen acts as a reference plane.

4.2.2 Initial setting of the mirror angle

To set the mirror angle position we have to calculate the back reflection angle 2ξ . This is calculated by adjusting the mirror and the grating angle to obtain a back reflection as shown in the figure below. Let θ_{ibr} & θ_{rbr} be the input & reflected angle at which the double-pass condition occurs.

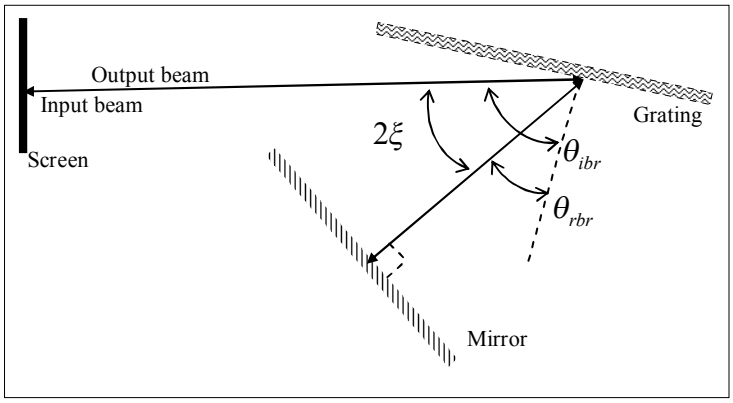

Figure 4.3: The back-reflection angle condition at which the reflected beam passes back along the normal to the mirror

From the figure,

$$2\xi = \theta_{ibr} - \theta_{rbr} \tag{4.1}$$

4.2.3 Rotation of the grating

Once the back reflection angles are set, the grating can be rotated to a new angle θ_{i1} which gives a new reflected angle θ_{r1}

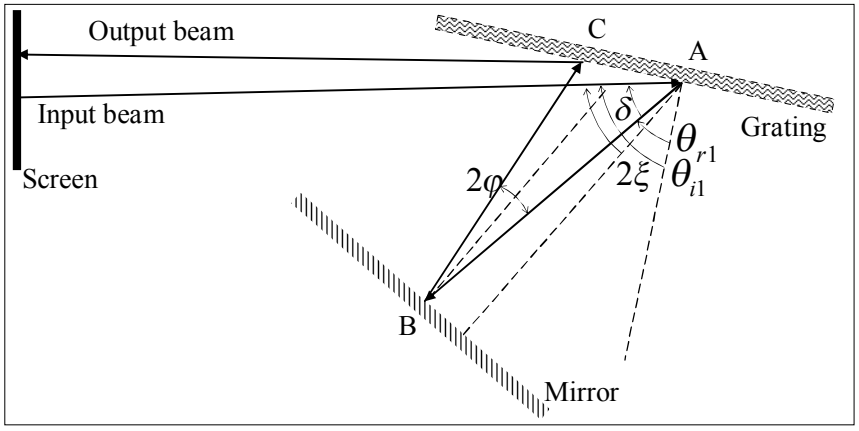

Figure 4.4: Side-view of the double-pass grating.

From Fig 4.4,

$$\delta = \theta_{i1} - \theta_{r1} \tag{4.2}$$

$$\varphi = 2\xi - \delta \tag{4.3}$$

4.2.4 Input Ray Matrix

The input ray matrix is given by

$$\begin{bmatrix} x_{in} \\ \theta_{in} \\ 1 \end{bmatrix} \tag{4.4}$$

Here the input elements are defined with respect to the input beam which is taken as the optical axis when the beam starts out.

4.2.5 Free space section, L1

The optical ray propagates through a distance L_1 before reaching the grating. The ray matrix of the ray after traveling through section L1 is given by,

$$\begin{bmatrix} x_{L1} \\ \theta_{L1} \\ 1 \end{bmatrix} = \begin{bmatrix} 1 & L_1 & 0 \\ 0 & 1 & 0 \\ 0 & 0 & 1 \end{bmatrix} \begin{bmatrix} x_{in} \\ \theta_{in} \\ 1 \end{bmatrix} \tag{4.5}$$

4.2.6 Grating G1

The output ray from the grating is given by (assuming no dispersion)

$$\begin{bmatrix} x_{G1} \\ \theta_{G1} \\ 1 \end{bmatrix} = \begin{bmatrix} A1 & 0 & 0 \\ 0 & D1 & 0 \\ 0 & 0 & 1 \end{bmatrix} \begin{bmatrix} x_{L1} \\ \theta_{L1} \\ 1 \end{bmatrix} \tag{4.6}$$

Where $A1 = \dfrac{\cos\theta_{r1}}{\cos\theta_{i1}}$ & $D1 = \dfrac{\cos\theta_{i1}}{\cos\theta_{r1}}$. The output vector is with respect to the reflected beam. It is desired to find the output slope and displacement w.r.t the normal of the mirror, since information will assist in finding out the deviation of the beam from the back-reflection condition. The ray matrix is modified by making its output angle relative to mirror normal,

$$\begin{bmatrix} x_{G1} \\ \theta_{G1} \\ 1 \end{bmatrix} = \begin{bmatrix} A1 & 0 & 0 \\ 0 & D1 & \theta_{gr1} \\ 0 & 0 & 1 \end{bmatrix} \begin{bmatrix} x_{L1} \\ \theta_{L1} \\ 1 \end{bmatrix} \tag{4.7}$$

Where $\theta_{gr1} = \varphi$ as shown in the figure below.

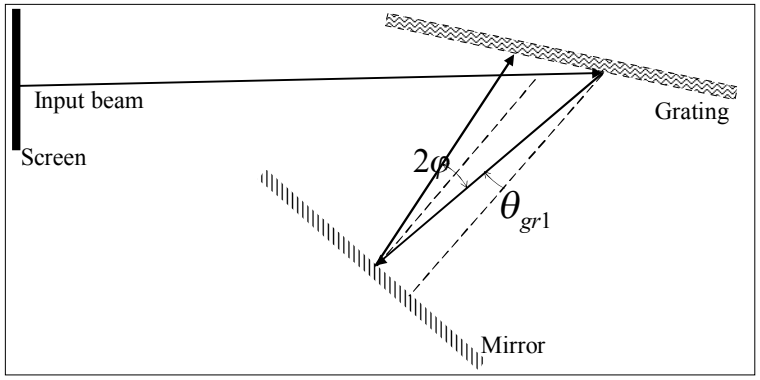

Figure 4.5: Deviated path of the ray from the mirror normal.

4.2.7 Free space section L2

The optical ray propagates through a distance L_2 from the grating to the mirror. The ray matrix of the ray after traveling through section L2 is given by,

$$\begin{bmatrix} x_{L2} \\ \theta_{L2} \\ 1 \end{bmatrix} = \begin{bmatrix} 1 & L_2 & 0 \\ 0 & 1 & 0 \\ 0 & 0 & 1 \end{bmatrix} \begin{bmatrix} x_{G1} \\ \theta_{G1} \\ 1 \end{bmatrix} \tag{4.8}$$

The output vector entering the mirror is relative to the normal to the mirror from the point of incidence of the input beam.

4.2.8 Mirror section M1

The ray is simply reflected off the mirror & the ray transfer matrix after reflection is still w.r.t the mirror normal & is given by,

$$\begin{bmatrix} x_{M1} \\ \theta_{M1} \\ 1 \end{bmatrix} = \begin{bmatrix} 1 & 0 & 0 \\ 0 & 1 & 0 \\ 0 & 0 & 1 \end{bmatrix} \begin{bmatrix} x_{L2} \\ \theta_{L2} \\ 1 \end{bmatrix} \tag{4.9}$$

4.2.9 Free space section L3

The optical ray propagates through a distance L_3 from the grating to the mirror. The ray matrix of the ray after traveling through section L3 is given by,

$$\begin{bmatrix} x_{L3} \\ \theta_{L3} \\ 1 \end{bmatrix} = \begin{bmatrix} 1 & L_3 & 0 \\ 0 & 1 & 0 \\ 0 & 0 & 1 \end{bmatrix} \begin{bmatrix} x_{M1} \\ \theta_{M1} \\ 1 \end{bmatrix} \tag{4.10}$$

The input vector from the mirror must be w.r.t the beam falling on the grating 2 & not w.r.t. to the mirror normal. Adjustments must be made to the output vector before it passes through the grating 2. The displacement is offset by distance AC & slope by angle of BC with the mirror normal.

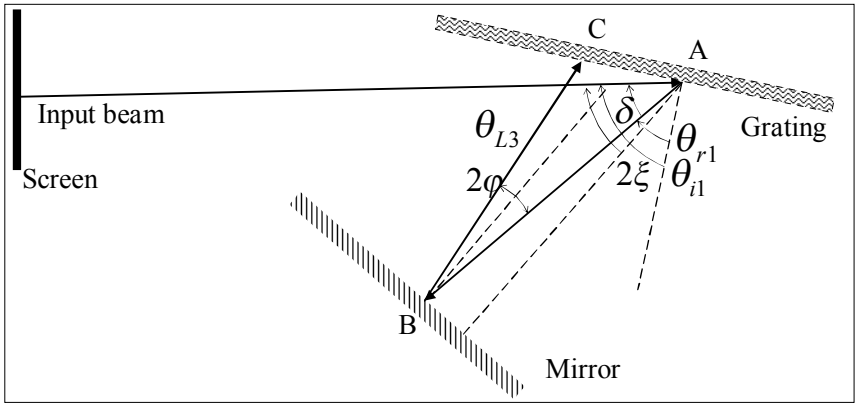

Figure 4.6: Angle of deviation of the ray from the mirror.

The ray matrix of the ray after traveling through section L3 is given by,

$$\begin{bmatrix} x_{L3} \\ \theta_{L3} \\ 1 \end{bmatrix} = \begin{bmatrix} 1 & L_3 & E_3 \\ 0 & 1 & F_3 \\ 0 & 0 & 1 \end{bmatrix} \begin{bmatrix} x_{M1} \\ \theta_{M1} \\ 1 \end{bmatrix} \tag{4.11}$$

Where $E_3 = -\left(L_2 + L_3\right)\theta_{gr1}$ offsets the distance traveled by the input vector & $F_3 = -\theta_{gr1}$ offsets the angle made w.r.t. the normal of the mirror.

4.2.10 Grating Section G2

The output ray vector w.r.t to the output beam is given by

$$\begin{bmatrix} x_{G2} \\ \theta_{G2} \\ 1 \end{bmatrix} = \begin{bmatrix} A2 & 0 & 0 \\ 0 & D2 & 0 \\ 0 & 0 & 1 \end{bmatrix} \begin{bmatrix} x_{L3} \\ \theta_{L3} \\ 1 \end{bmatrix} \tag{4.12}$$

It is desirable to get the output ray vector w.r.t. the input beam, this enables us to compare the slope & position of the output beam w.r.t input beam. Adjustments need to be made.

$$\begin{bmatrix} x_{G2} \\ \theta_{G2} \\ 1 \end{bmatrix} = \begin{bmatrix} A2 & 0 & E_{gr2} \\ 0 & D2 & F_{gr2} \\ 0 & 0 & 1 \end{bmatrix} \begin{bmatrix} x_{L3} \\ \theta_{L3} \\ 1 \end{bmatrix} \tag{4.13}$$

Here $A2 = \dfrac{\cos\theta_{r2}}{\cos\theta_{i2}}$ & $D2 = \dfrac{\cos\theta_{i2}}{\cos\theta_{r2}}$ where $\theta_{i2} = \theta_{r1} - 2\varphi$

$$E_{gr2} = -E_3\left(\frac{\pi}{2} - \theta_{i1}\right) \text{ \& } F_{gr2} = \left(\theta_{i1} - \theta_{r2}\right)$$

4.2.11 Free space section L4

The output ray vector w.r.t to the input beam is given by

$$\begin{bmatrix} x_{L4} \\ \theta_{L4} \\ 1 \end{bmatrix} = \begin{bmatrix} 1 & L_4 & 0 \\ 0 & 1 & 0 \\ 0 & 0 & 1 \end{bmatrix} \begin{bmatrix} x_{G2} \\ \theta_{G2} \\ 1 \end{bmatrix} \tag{4.14}$$

4.3 Putting it all together

The total effect of all the elements on the transformation of the input beam as it passes through the system is given by the matrix multiplication of the input vector with all the matrices of the elements it encounters i.e.

$$[OP] = [L4][G2][L3][M1][L2][G1][L1][IN] \tag{4.15}$$

The final equations of the output matrix are

$$\begin{bmatrix} x_{L4} \\ \theta_{L4} \\ 1 \end{bmatrix} = \begin{bmatrix} A1\,A2 & D2\left(A1\left(L_1+L_3\right)+D1\,L_2\right)+A1\,A2\,L_4 & A1\left(E_3+E_{gr2}\right)+F_3\left(A1\,L_1+D1L_2\right)+F_{gr2}\left(A1\left(L_1+L_3\right)+D1L_2\right)+L_2\theta_{gr1} \\ 0 & D1\,D2 & D1\left(F_3+F_{gr2}\right)+\theta_{gr1} \\ 0 & 0 & 1 \end{bmatrix} \begin{bmatrix} x_{in} \\ \theta_{in} \\ 1 \end{bmatrix} \tag{4.16}$$

Simplifying (4.16) and expressing it in terms of it individual vector elements we get,

$$\begin{aligned} x_{L4} &= A1\,A2\cdot x_{in} \\ &+\left(D2\left(A1\left(L_1+L_3\right)+D1\,L_2\right)+A1\,A2\,L_4\right)\cdot\theta_{in} \\ &+A1\left(E_3+E_{gr2}\right)+F_3\left(A1\,L_1+D1L_2\right)+F_{gr2}\left(A1\left(L_1+L_3\right)+D1L_2\right)+L_2\theta_{gr1} \end{aligned} \tag{4.17}$$

$$\theta_{L4} = D1\,D2\cdot\theta_{in}+D1\left(F_3+F_{gr2}\right)+\theta_{gr1} \tag{4.18}$$

Assuming the input vector to have a value of [0, 0, 1] i.e. the input ray starts at the origin (beginning of the screen) and the optical axis is the path of the input beam and substituting the values of E_3, F_3, E_{gr2}, F_{gr2} as defined in the previous sections we get

$$\begin{bmatrix} x_{L4} \\ \theta_{L4} \\ 1 \end{bmatrix} = \begin{bmatrix} A2\,L1\cdot\theta_{gr1} \\ \left(A2L_2L_4+D2\left(1+L_2L_3\right)\right)\cdot\theta_{gr1} \\ 1-\theta_{gr1}^2+L_2\left(L_2+L_3\right)\theta_{gr1}^2\left(1+\frac{\pi}{2}\theta_{i1}\right)+\theta_{gr1}\left(1+L_2L_3\right)\left(\theta_{i1}-\theta_{r2}\right) \end{bmatrix} \tag{4.19}$$

Now if the grating is exactly at the double-pass position then $\theta_{gr1} = 0$. (4.19) then reduces to [0, 0, 1]. This means that the output ray is equal to the input ray i.e the output ray passes along the optical axis and the reference plane of the input ray.

CHAPTER 5

MEASUREMENT SETUP & PROCEDURE

5.1 Introduction

This section shows the procedure to measure the modes of the laser diode. The initial adjustments of the elements are explained. The procedure of performing the measurement & acquisition of the modes of the laser diodes using the computer is explained. The optical power measurement is also explained.

5.2 Initial adjustments

These are steps taken before any measurement of the spectra is started. This is mainly to ensure the laser is properly focused & the path is properly aligned.

5.2.1 Laser diode mounting

The laser diode is carefully attached to the laser diode mount using a screw driver. It is aligned such that the stripe facet is in the horizontal direction. This mount is then placed on a translation stage. The translation stage can be adjusted in 3 dimensions & also for angular adjustment in the horizontal direction.

After placing it on the alignment stage, it is then soldered to the power supply wires & the water cooling system is turned on.

5.2.2 Adjustments of the optical setup

Before attempting to switch on the laser diode, the eyes should be protected using appropriate laser safely goggles. This is extremely important to prevent injury to the eyes due to an accident or stray reflection of light falling on the eye. In order to prevent the effect of stray light, the experiment is performed under low-light conditions.

The power supply is turned on & the voltage is increased until the current is just around the threshold value, this is indicated by a surge in the value of the current on the power supply reading. The laser diode is checked for light using a laser beam detection card. Once there is light, the focusing lens is adjusted to focus the beam on the output such that there it has a uniform dimension falling on the polarizer. The polarizer is adjusted to get a linear polarized beam which has maximum intensity.

The beam from the polarizer goes into a collimating lens. The distance between the laser diode & the collimating lens is adjusted to be equal to the distance between the collimating lens & the slit. This distance is the focal distance of the collimating lens. This is done to ensure the beam is in focus.

This beam is passed through a half-wave plate to get the desired orientation of the beam. This beam is then passes through a slit. The slit is used to control the intensity of the beam & is adjusted to obtain a narrow beam.

The output from the slit is passed on to the grating through a collimating lens. The collimating lens is placed such that the distance from the slit to the lens is equal to the distance traveled by the beam from the lens through the double-pass grating & back to the lens. This ensures the beam is in proper focus when it enters & leaves the grating.

The rotation stage controller is now put ON. The position is of the controller is reset to the initial position. The grating is tilted to the double-pass angle condition using the computer program. As seen from Figure, the speed of the rotation stage can also be controlled by the computer program.

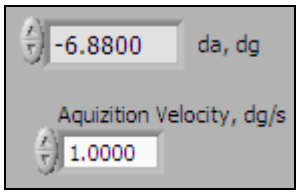

Figure 5.1: Interface of LABVIEW program to control the rotational stage.

The double-pass mirror distance from the grating is adjusted to ensure the focusing condition of the collimating lens is met. The diffracted beam leaving the grating is passed through the same collimating lens as the one it came through. It is sent into the Near-field/Far-field Optical System (NFFFOS). The NFFFOS elements must be adjust such that the two beam spots are directly focused onto the linear Si Charge Coupled Device (CCD) camera lens.

5.3 Measurement procedure

5.3.1 LabVIEW Calibration

Once the initial setup is done, the TV monitor is switched on. The output of the laser beam is observed on the TV & the setup can be further refined to get a clear focused image of the beam in the middle of the CCD lens.

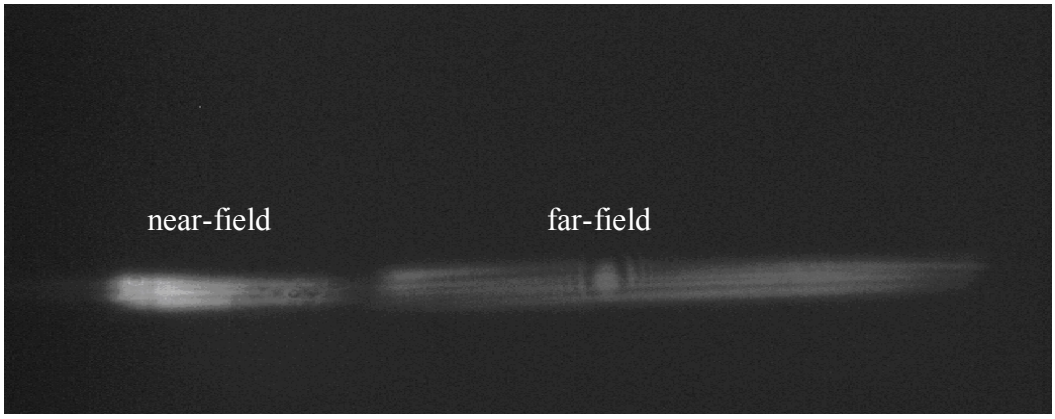

Figure 5.2: The near-field & far-field of the laser beam during calibration process

Once this is done, the LabVIEW calibration program is executed. The setup of the calibration program interface is as shown in the figure below. Once it is complete, it outputs the calibration data into a text file.

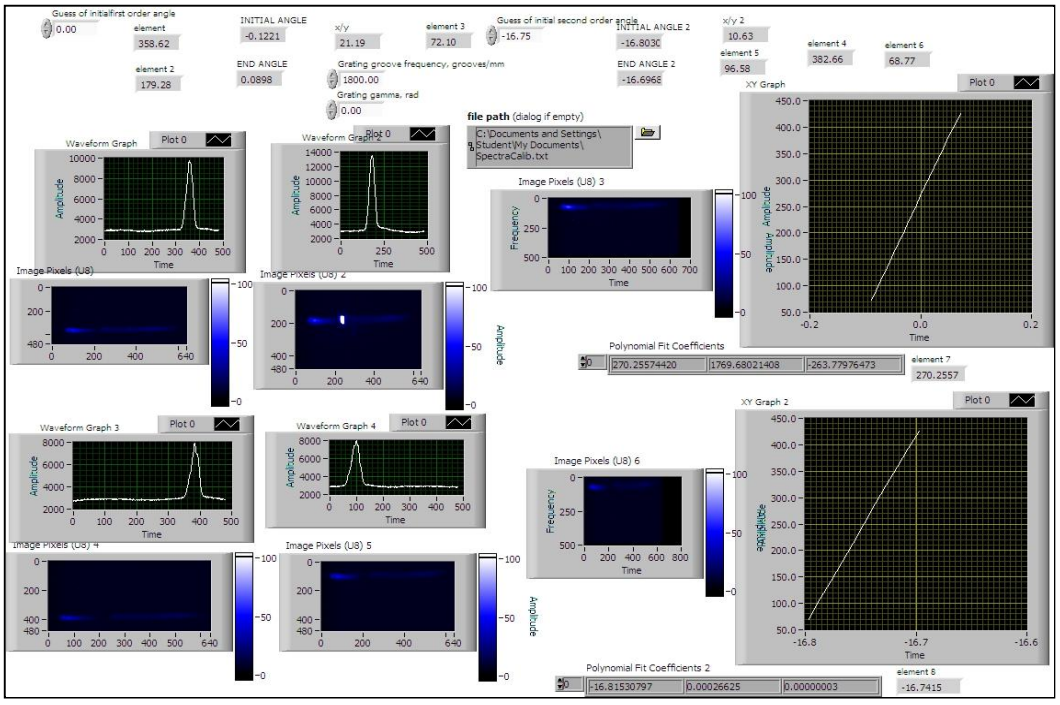

Figure 5.3: The interface of the grating setup calibration process

5.3.2 Main spectrum scan

The main spectrum scan program is now run. This rotates the grating at various angles & captures the spectra. The input parameters to this program are the grating period & the center wavelength. The program takes the calibration results from the text file generated by the previous program.

Once the program is run, it asks for the minimum spectral range cutoff. This is determined by manually adjusting the grating angle using the controller. We find the minimum angle at which the modes are visible. It then asks for the maximum spectral range. We similarly adjust the grating angle towards the maximum until the modes just about disappear. Once the minimum and maximum spectral values are obtained, the program asks for the light beam to be blocked. This can be done manually. This is done to measure the background noise of the CCD. It then asks for the block to be opened to conduct the measurement.

The measurement time depends on the spectral range and takes anywhere between 2 minutes to 10 minutes. The images are then resampled and stitched together using the dispersion formula of the spectrometer i.e. parabolic interpolation [3.2].

As seen in Fig 5.4, the acquired spectra consists of the near-field on the left & the far-field on the right. The y-axis is common and is the wavelength of the light. The x-axis consists of the position of the near-field & angular spread for the far-field.

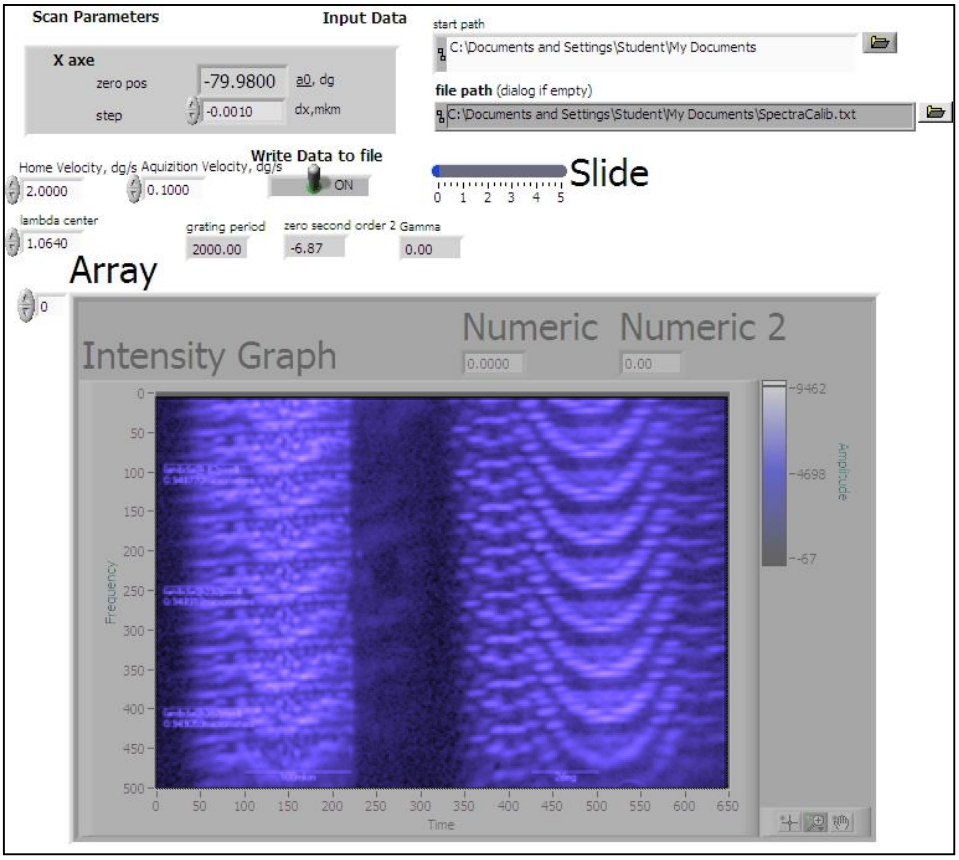

Figure 5.4: The interface of the main program which scans the spectrum and converts to it to individual images.

5.3.3 Power Measurement of the BALD

Power meter is used to calculate the output power of the BALD for different values of current. The quantum efficiency of the BALD can be calculated from the measurements.

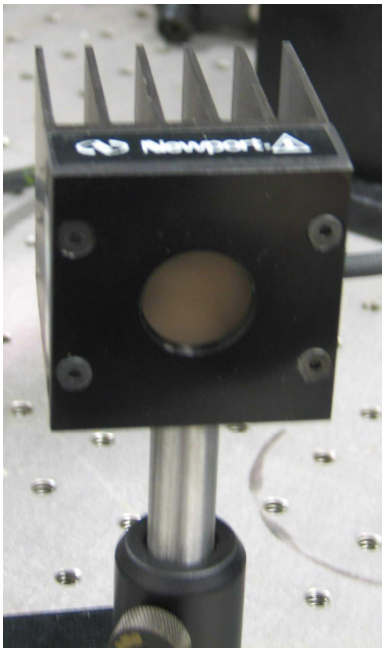

Fig 5.5: Power meter is used to calculate the output power of the BALD for different values of current.

The measurement results are shown in Table 5.1. I is the measured current in mA, The $I_{corrected}$ is the corrected value of the measured current from the power meter. P0 is the power meter reading in mW when it is closed i.e. without any input. P_{open} is the power meter reading when it is open and the laser is incident on it. Diff is the actual power reading.

Table 5.1: The power measurement values of the BALD

I(mA)	Icorrected (mA)	P0(Mw)	Popen(mW)	Diff(mW)
400	406	1.7	55.5	53.8
800	806	1.7	201	199.3
1000	1006	1.5	290	288.5
1500	1506	1.1	442	440.9
2000	2006	0.3	590	589.7
2500	2506	0.8	882	881.2
3000	3006	0.3	983	982.7
3500	3506	0.5	1119	1118.5
4000	4006	0.8	1300	1299.2
4500	4506	0.5	1551	1550.5
5000	5006	0.6	1643	1642.4
5500	5506	0.6	1875	1874.4
6000	6006	0.5	1954	1953.5
7000	7006	0.9	2250	2249.1
8000	8006	0.8	2370	2369.2

Plotting the above values, we get the graph,

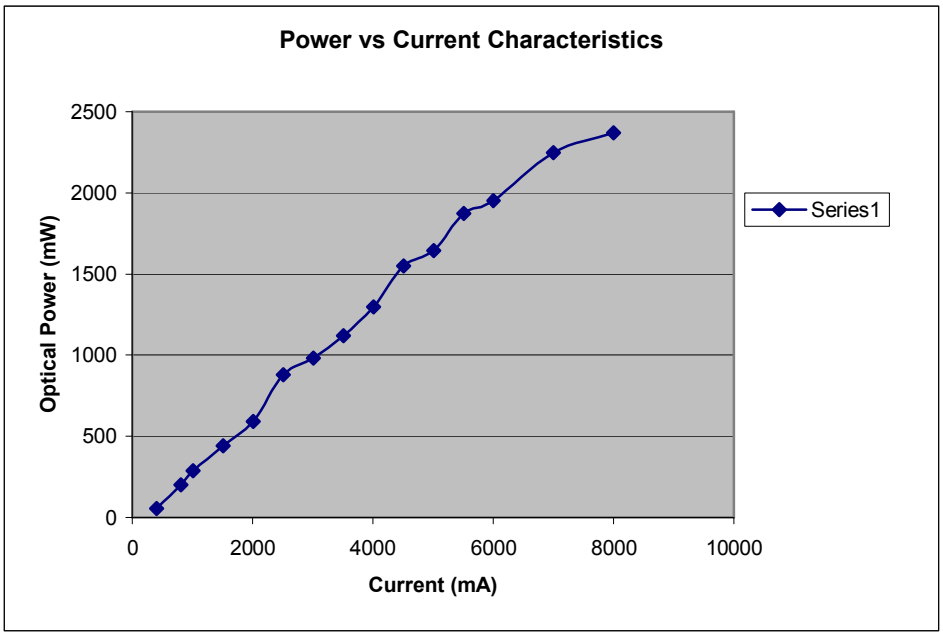

Fig 5.6: Power measurement graph of the BALD@20 deg.

CHAPTER 6

RESULTS AND CONCLUSION

6.1 Results

The following image sets were captured for increasing values of current. The output spectra is shown as the grating angle is varied at a particular value of current. The modes are spread across the spectral range.

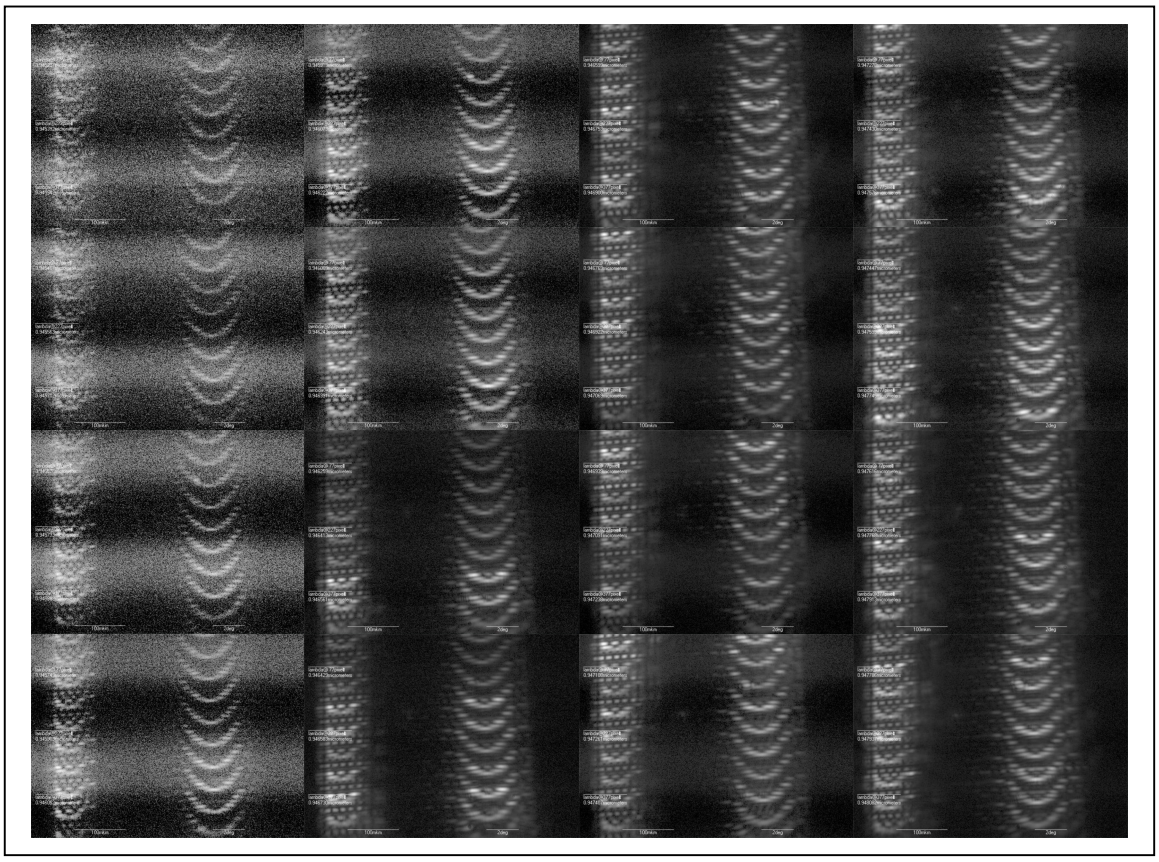

Fig 6.1: Near-field/far-field output spectra of BALD@ 20 deg /400mA/Strip width: ~100µm with increasing wavelength from top to bottom and left to right.

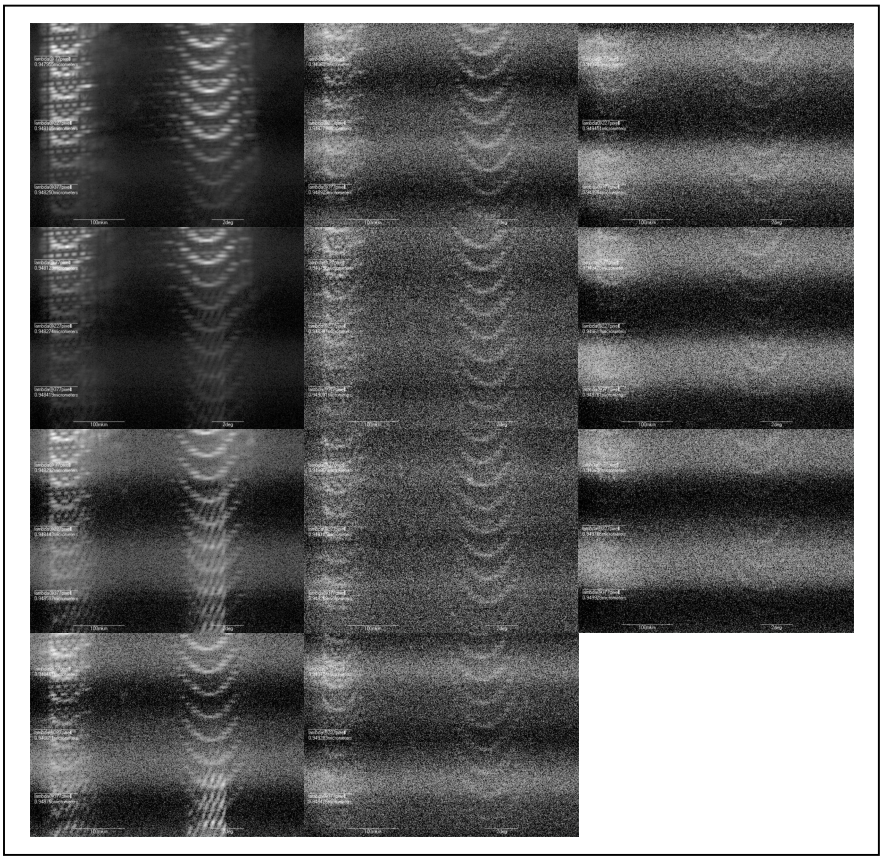

Fig 6.2: Near-field/far-field output spectra of BALD@ 20 deg /400mA/ Strip width: ~100μm with increasing wavelength from top to bottom and left to right.

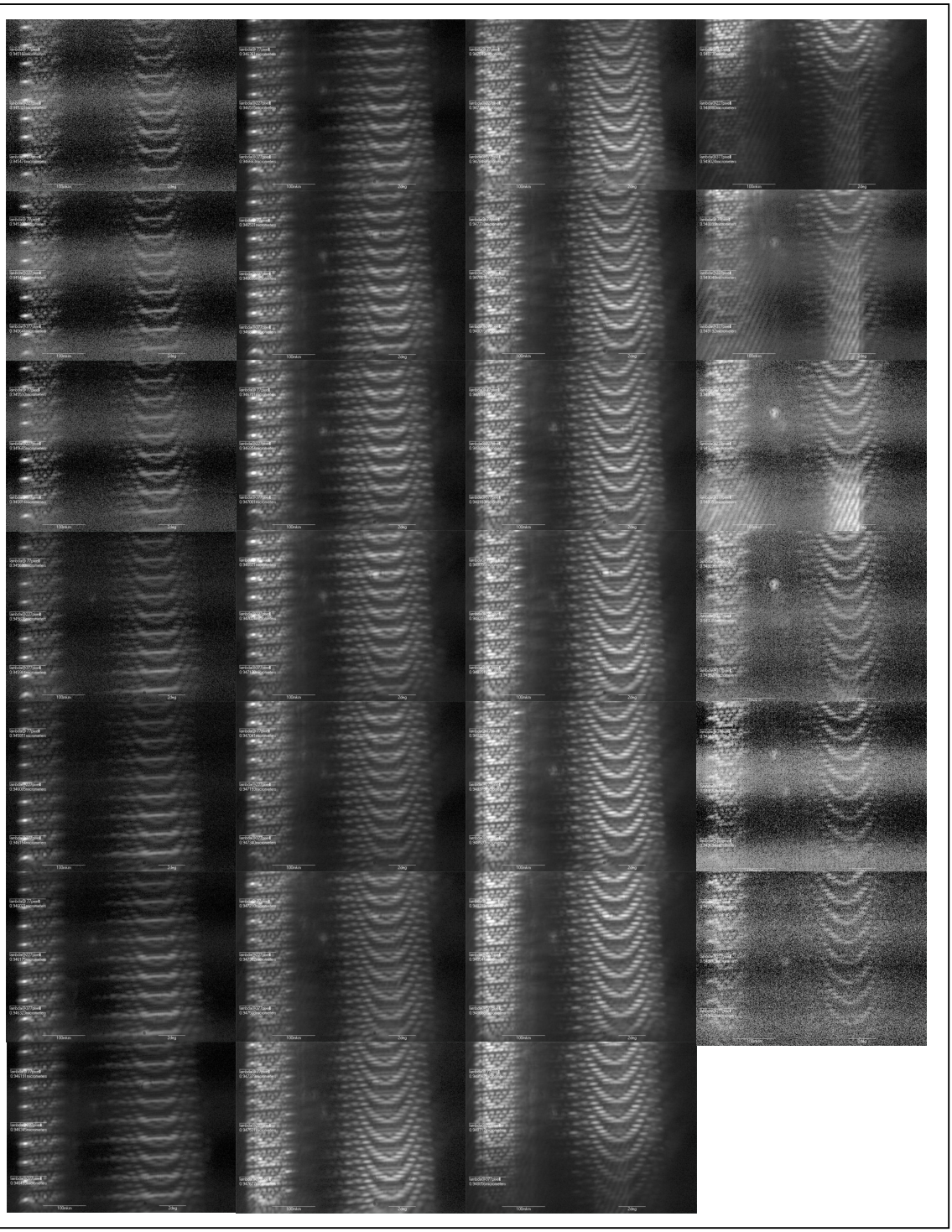

Fig 6.3: Near-field/far-field output spectra of BALD@ 20 deg /1000mA/ Strip width: ~100μm with increasing wavelength from top to bottom and left to right.

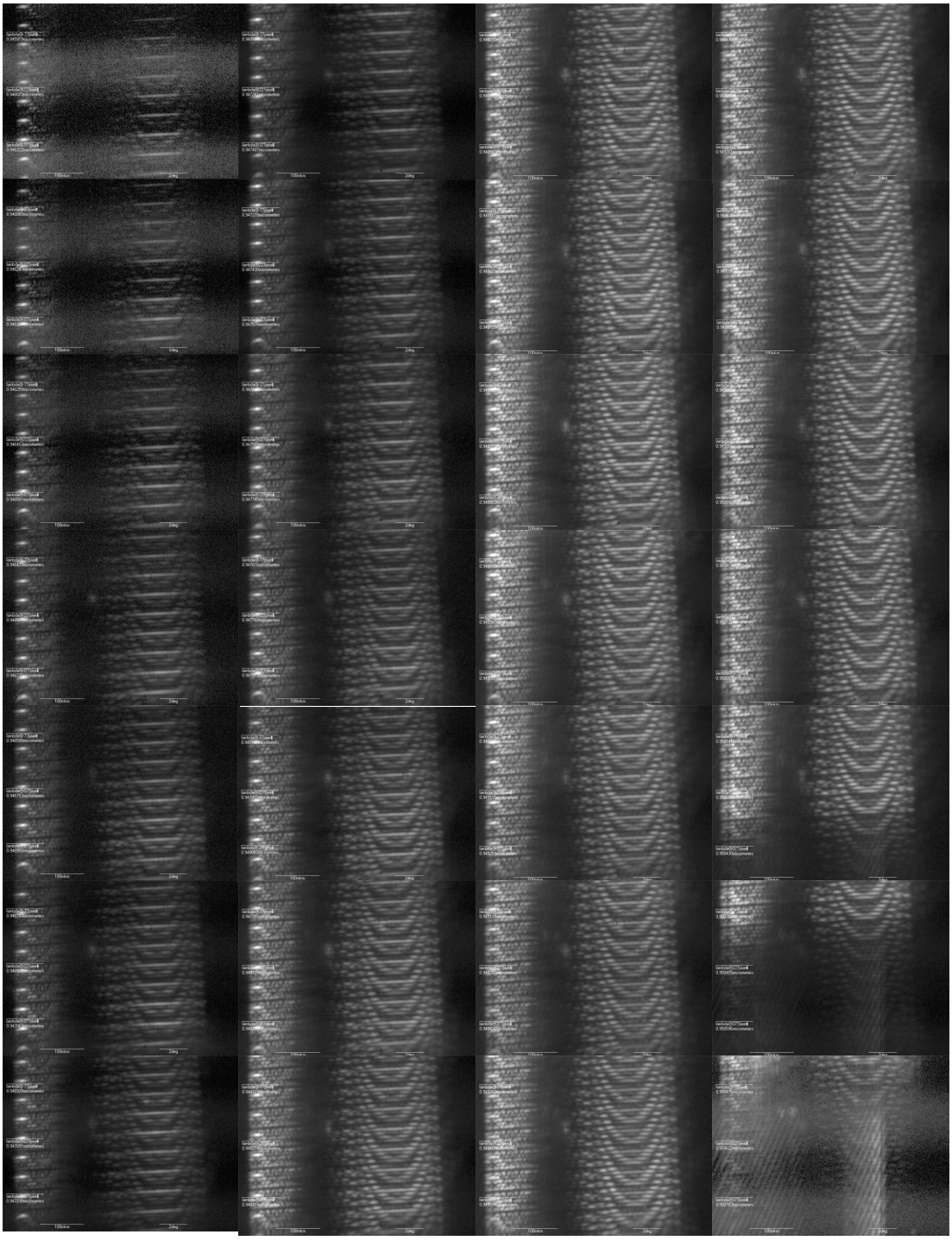

Fig 6.4: Near-field/far-field output spectra of BALD@ 20 deg /2000mA/ Strip width: ~100μm with increasing wavelength from top to bottom and left to right.

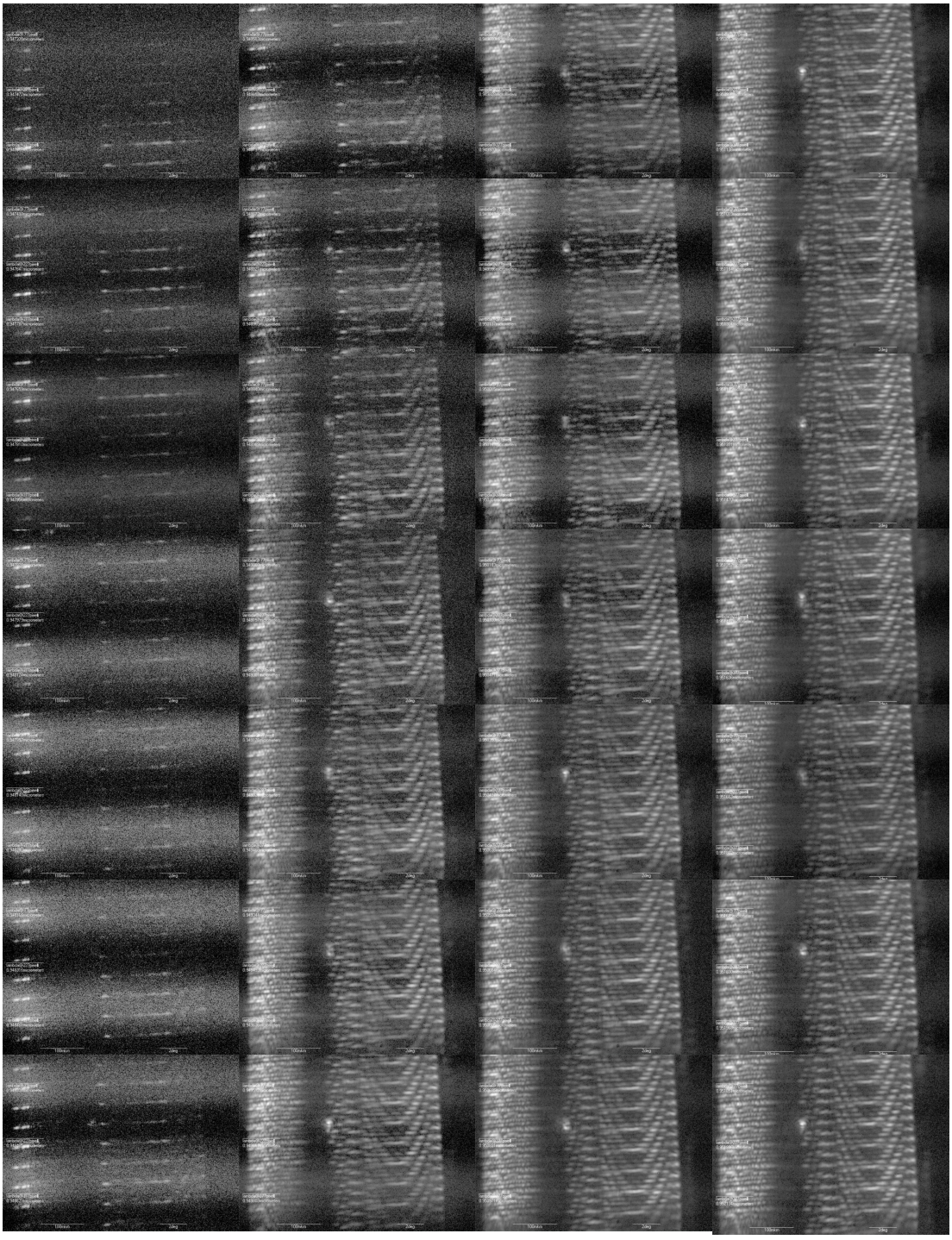

Fig 6.5: Near-field/far-field output spectra of BALD@ 20 deg /4000mA/ Strip width: ~100μm with increasing wavelength from top to bottom and left to right.

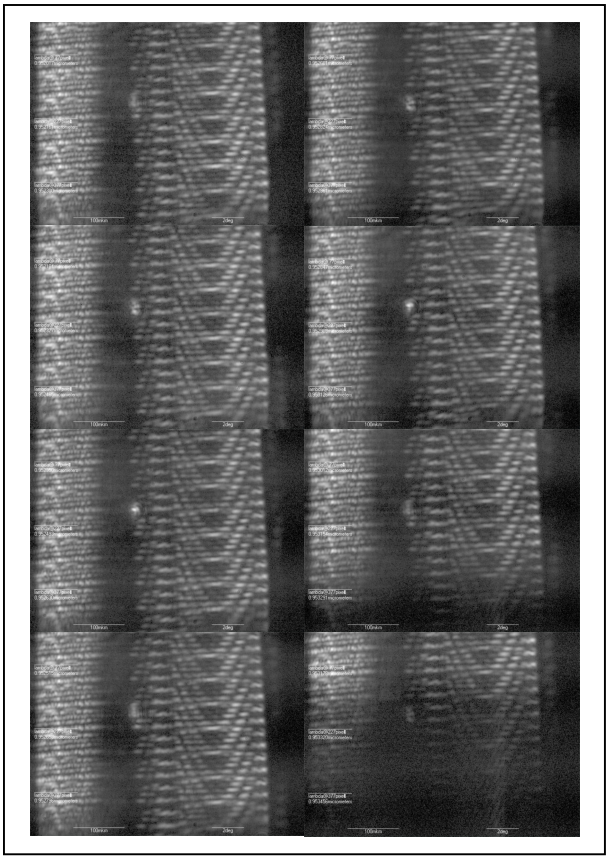

Fig 6.6: Near-field/far-field output spectra of BALD@ 20 deg /4000mA/ Strip width: ~100μm with increasing wavelength from top to bottom and left to right.

6.2 Conclusion

The theory of the double-pass spectrometer was explained and the setup to record and capture the modes of the laser diode using labview software. The following images were captured for increasing values of current and also the power output. The modes of the laser diode are clearly visible. They are spread spectrally in the near & far-field. The profile of the mode structure matches the profile of the gain guided dielectric slab waveguide.

CHAPTER 7

FUTURE WORK

7.1 Future work

As with every test instrument, the aim would be have a completely automated double-pass spectrometer setup to increase efficiency & speed of testing.

Many of the manual adjustments & calibrations, like noting the minimum & maximum position of the spectra, closing the slit, etc. can be automated to make each test faster. The calculation of the position and power intensity of each mode could be done in automated manner.

Another improvement would be to merge the entire set of images into one full image to show the full variation across lateral space. Right now as the grating rotates, snapshots of across different lateral widths are taken. This leads to many individual images.

The effect of triple-pass & quadruple-pass on the resolution of the output spectra can also be investigated.

The effect of the output spectra for different values of the angle γ, the rotational angle of the grating in the plane parallel to the grating grooves needs to be studied in greater detail.

Using advanced optical systems design, the space required by the setup can be reduced. This leads to a more compact & flexible setup. The positioning of several components could be automated i.e. control of the position of lens by mechanized stage.

Using the matrix model to find the change in position of the beams from the initial condition & linking this to the software, we could have more control over the system.

APPENDIX A

REVIEW OF MATRIX OPTICS

A.1 Introduction

The theory of matrix optics is introduced. The ray transfer matrix of various optical elements is defined & the paraxial propagation of geometrical optical rays through them is described & modeled.

A.2 Matrix methods in optics

The optics of paraxial imaging [4.1] is often referred to as Gaussian optics. Gauss showed that the behavior of any lens system can be determined from knowledge of its six cardinal points - namely two focal points, two nodal points of unit angular magnification & two principal points of unit linear magnification. In formulating the latter, Gauss wrote down explicitly the two linear simultaneous equations whereby the ray height & ray angle of an output ray are linked to the corresponding quantities for an input ray.

Matrices provide an alternative method for performing this type of calculation. It would seem that they were first used in optics by Sampson about sixty years ago, but it is only recently that they have been widely adopted.

During 1965 Kogelnik published an important extension of the method whereby a ray-transfer matrix could be used to describe not only the geometric optics of paraxial rays but also the propagation of a diffraction- limited laser beam.

A.2.1 Assumptions of matrix method

The first is the basic assumption of all geometric optics - that the wavelength of light is negligibly small & that propagation of light can be described not in terms of

wavefronts but in terms of individual rays. The concept of a geometric ray is an idealization of this normal to the wavefront.

The second approximation is that rays are assumed to be paraxial - those that remain close to the axis & almost parallel to it so that the first-order approximations for the sines or tangents of any angles that are involved. This method will therefore give no information about third-order effects such as spherical aberration or the oblique aberrations coma, astigmatism, field curvature & distortion.

A.2.2 Optical ray definition

Consider a ray of light [4.2] traveling approximately in the z direction. Let us define a reference plane z_1 that is perpendicular to the optical axis. Let the ray travel with a transverse displacement of r from the optical axis to the reference plane. (where r is a function of z). Let this ray make a small slope of $r' = dr/dz$ with the optical axis as shown in Fig A.1

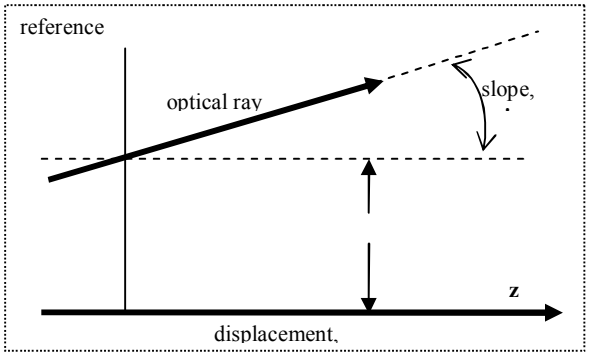

Figure A.1: The optical ray is defined in terms of the displacement r from the optical axis to the reference plane z_1 and the slope r' it makes with respect to the optical axis.

A.2.3 Optical ray transformation

Let an optical ray propagate in free space from one plane z_1 to another plane z_2 at a distance L from z_1 as show in Figure A.2.

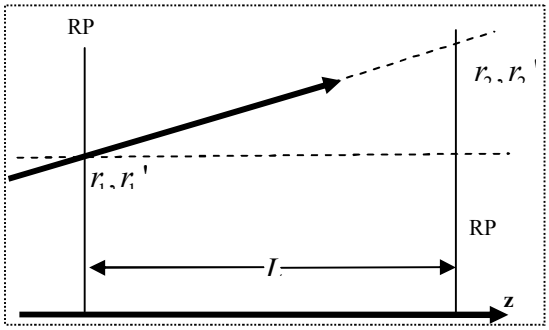

Figure A.2: Optical ray passing from plane z_1 to plane z_2 is transformed in term of its displacement r and slope r'.

The ray is now describes by these co-ordinates i.e. its displacement & slope with respect to the optical axis for a particular reference plane. Let the co-ordinates at the input plane z_1 be r_1, r_1' & let the co-ordinates at the output plane z_2 be r_2, r_2'. These co-ordinates are related by the transformation

$$r_2 = r_1 + L\, dr_1 / dx \tag{D.20}$$

$$dr_2 / dx = dr_1 / dx \tag{D.21}$$

As seen from the above equations, the input & output co-ordinates are by related by linear transformations. The output displacement & slope of an optical ray passing through a wide variety of optical elements can also be represented in a similar manner.

To simplify [4.2] the later results of the transformations, we define the ray slope variable to be the actual slope dr/dz of the ray multiplied by the local index of refraction $n(z)$ at the ray position. This quantity is known as the reduced slope given by

$$r'(z) = n(z)\frac{dr(z)}{dz} \tag{D.22}$$

A.2.4 ABCD matrices

The matrix representation of an optical element is generally referred to as ABCD matrix. We represent the output displacement & slope as a linear combination of the input.

$$\begin{aligned} r_2 &= Ar_1 + Br_1' \\ r_2' &= Cr_1 + Dr_1' \end{aligned} \tag{D.23}$$

where the coefficients A, B, C & D characterize the paraxial focusing properties of this element.

The idea is to construct a matrix M which represents an optical element through which the ray will pass. Figure A.3 shows a typical optical system with various optical elements & the path of the optical ray through it.

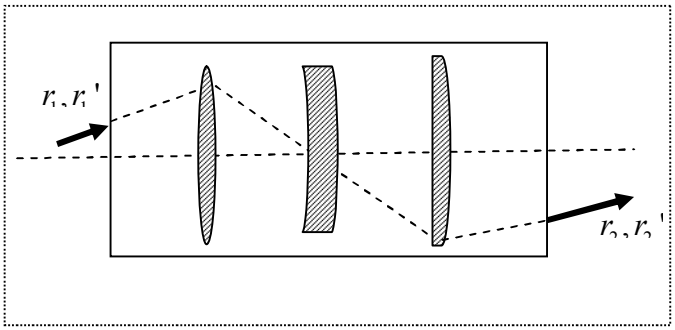

Figure A.3: Optical ray passing through various optical elements.

An optical element can be represented by a matrix M where the output of the ray can be determined by linear transformation of the input by several optical elements. This is show in Figure A.A.

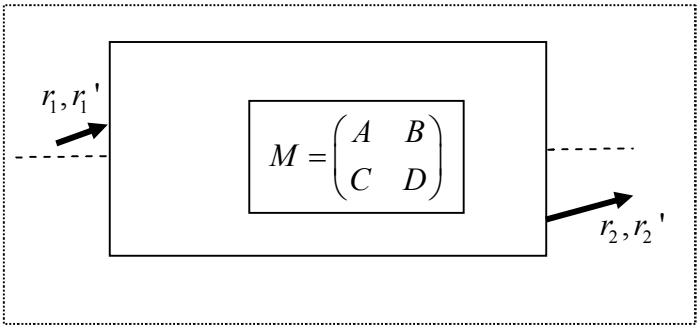

Figure A.4: A matrix M can be used to represent each optical element as the ray propagates through the system.

Hence we can write Equation (A.4) as

$$\mathbf{r}_2 \equiv \begin{bmatrix} r_2 \\ r_2' \end{bmatrix} = \begin{bmatrix} A & C \\ B & D \end{bmatrix} \times \begin{bmatrix} r_1 \\ r_1' \end{bmatrix} \equiv \mathbf{M}\,\mathbf{r}_1 \tag{D.24}$$

Since we have used the reduced slope definition of Equation (A.3), the determinant of the matrix **M,** $AD - BC = 1$. Otherwise it would be $AD - BC = n_1 / n_2$ where n1 & n2 are the refractive indices at the input & output planes.

A.2.5 Ray matrices for cascaded optical elements

In a typical optical system, elements are often arranged in a cascade i.e. a lens, free-space section, a thick lens, free-space section. Each of these can be represented by a matrix $\mathbf{M}_1, \mathbf{M}_2, ...\mathbf{M}_n$. The state of the input ray at the plane between two optical elements is shown in Figure A.5

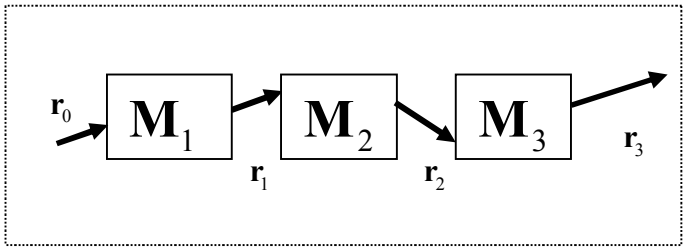

Figure A.5: The cascaded system of optical elements represented as matrices and the effect of the input ray through them.

The transformation of the input ray as it passes through the system is given by

$$\begin{aligned} \mathbf{r}_1 &= \mathbf{M}_1\mathbf{r}_0 \\ \mathbf{r}_2 &= \mathbf{M}_2\mathbf{r}_1 = \mathbf{M}_1\mathbf{M}_0\mathbf{r}_0 \\ \mathbf{r}_3 &= \mathbf{M}_3\,\mathbf{r}_2 = \mathbf{M}_3\mathbf{M}_2\mathbf{M}_1\mathbf{r}_0 \end{aligned} \tag{D.25}$$

In general the total effect of all the elements of the system on the input ray is given by

$$\mathbf{r}_n = [\mathbf{M}_n\mathbf{M}_{n-1}\mathbf{M}_{n-2}...\mathbf{M}_1]\mathbf{r}_0 = \mathbf{M}_{total}\mathbf{r}_0 \tag{D.26}$$

A.2.6 Ray matrices for misaligned elements

The 2 X 2 matrix formalism is developed under the assumption that all the paraxial elements are properly aligned and centered with respect to the reference axis. In order to account for misalignment in displacement & slope of the optical axis of the element with respect to the reference optical axis of the system, the matrix is expanded into a 3 X 3 matrix. An "error vector" **E** is added to optical element matrix along with a dummy element of unity to each of the ray vectors. The error vector **E** consists of quantities E & F which represent the displacement & slope misalignment respectively. The final equation of the 3 X 3 formalism is given by

$$\begin{bmatrix} r_2 \\ r_2' \\ 1 \end{bmatrix} = \begin{bmatrix} A & B & E \\ C & D & F \\ 0 & 0 & 1 \end{bmatrix} \times \begin{bmatrix} r_1 \\ r_1' \\ 1 \end{bmatrix} \tag{D.27}$$

A.2.7 Elements oftion grating matrix

A.3 Matrix representation of optical elements

The matrix representation of several optical elements is given below.

A.3.1 Free space section

Consider an optical ray propagating through free space from input plane z_1 to output plane z_2. If the free space section has a length L & refractive index n_0 then the matrix will be given by [4.1]

$$\begin{bmatrix} 1 & L/n_0 \\ 0 & 1 \end{bmatrix} \tag{D.28}$$

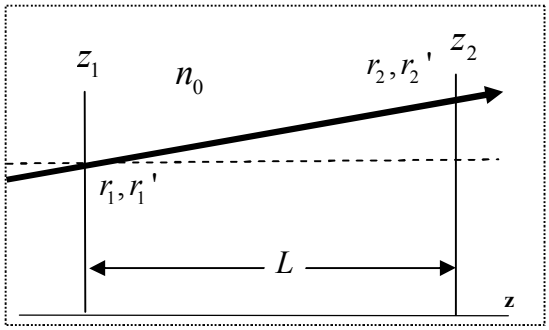

Figure A.6: Diagram for free space section

A.3.1 Free space section

Consider an optical ray propagating through free space from input plane z_1 to output plane z_2. If the free space section has a length L & refractive index n_0 then the matrix will be given by [4.1]

$$\begin{bmatrix} 1 & L/n_0 \\ 0 & 1 \end{bmatrix} \tag{D.29}$$

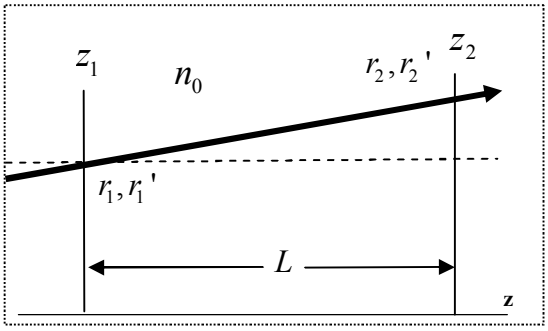

Figure A.6: Diagram for free space section

So the final equation for the case of 3X3 matrix will be of the form

$$\begin{bmatrix} r_2 \\ r_2' \\ 1 \end{bmatrix} = \begin{bmatrix} 1 & L/n_0 & E \\ 0 & 1 & F \\ 0 & 0 & 1 \end{bmatrix} \times \begin{bmatrix} r_1 \\ r_1' \\ 1 \end{bmatrix} \tag{D.30}$$

A.3.2 Curved Mirror

Similarly for a optical ray falling on a curved mirror, the ray matrix is given by [4.2]

$$\begin{bmatrix} 1 & 0 \\ 2/R_e & 1 \end{bmatrix} \tag{D.31}$$

where $R_e = R\cos\theta$ in the plane of incidence ('tangential') & $R_e = R/\cos\theta$ perpendicular to the place of incidence ('sagittal'). R is the angle of curvature of the mirror.

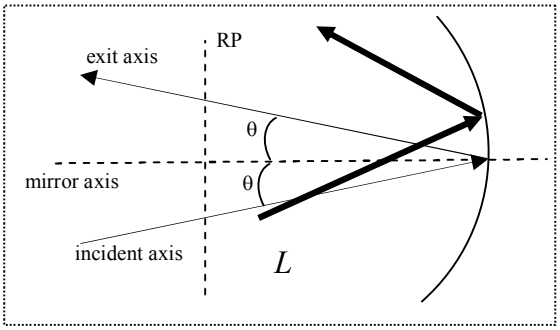

Figure A.7: Diagram for a curved mirror

Here the input ray vector is measured [A.1] with respect to the incident axis & the output ray vector is measured with respect to the exit axis.

APPENDIX B

MATRIX REPRESENTATION OF DIFFRACTION GRATING

B.1 Introduction

The matrix representation of the diffraction grating is explained & the matrix representation is compared with the exact equation of the diffraction grating.

B.2 The ray matrix of the diffraction grating

Assume we have a curved diffraction grating [B.1] as shown in Figure 1. Let the radius of curvature be R_g, the incident wave make an angle θ_1 with the grating normal, the diffracted wave make an angle θ_2 with the normal. Let the groove distance by d.

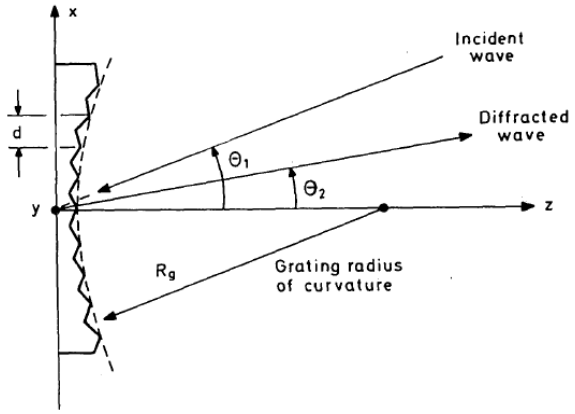

Figure B.1: The curved diffraction grating diagram used to develop the ray matrix. [B.1]

The diffraction grating equation is given by

$$\sin\theta_1 + \sin\theta_2 = \frac{m\lambda}{d} \tag{D.32}$$

where m is the diffraction order.

The ray matrix of the diffraction grating is of the form given by [B.2]

$$\begin{bmatrix} x_2 \\ x_2' \end{bmatrix} = \begin{bmatrix} A & B \\ C & D \end{bmatrix} \begin{bmatrix} x_1 \\ x_1' \end{bmatrix} \tag{D.33}$$

From Figure B.2, A is defined to be the [B.1] transverse magnification or the beam width expansion along the x-z plane given by

$$A=\frac{\cos\theta_2}{\cos\theta_1} \tag{D.34}$$

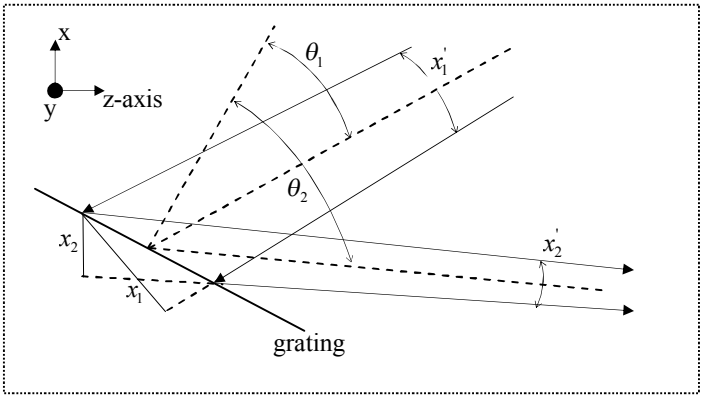

Figure B.2: The orientation of the input & output beam on the diffraction grating & the beam width expansion along the x-z axis. [B.3]

D is defined to be angular magnification given by

$$D=\frac{\cos\theta_1}{\cos\theta_2} \tag{D.35}$$

C is dependent on the radius of curvature R_g. In the transverse plane, C is given by

$$C=-\frac{2}{R_{gt}} \tag{D.36}$$

where $R_{gt}=-\frac{2\cos\theta_1\cos\theta_2}{\cos\theta_1+\cos\theta_2}R_g$. In the sagittal plane, C is given by

$$C=-\frac{2}{R_{gs}} \tag{D.37}$$

Where $R_{gs} = \dfrac{2}{\cos\theta_1 + \cos\theta_2} R_g$

For the double-pass grating we assume $R_g = 0$. Therefore the grating matrix is given by

$$\begin{bmatrix} x_2 \\ x_2^{'} \end{bmatrix} = \begin{bmatrix} \dfrac{\cos\theta_2}{\cos\theta_1} & 0 \\ 0 & \dfrac{\cos\theta_1}{\cos\theta_2} \end{bmatrix} \begin{bmatrix} x_1 \\ x_1^{'} \end{bmatrix} \tag{D.38}$$

B.3 The diffraction grating ray matrix including the angular frequency dispersion

Spectral angular dispersion can be developed & added by making use of the properties of the misaligned elements of the ABCD 3X3 matrix [B.2]

$$\begin{bmatrix} x_2 \\ x_2^{'} \\ 1 \end{bmatrix} = \begin{bmatrix} A & B & E \\ C & D & F \\ 0 & 0 & 1 \end{bmatrix} \begin{bmatrix} x_1 \\ x_1^{'} \\ 1 \end{bmatrix} \tag{D.39}$$

Here the misalignment terms E & F will be used to describe the spectral angular dispersion. The following assumptions are made [B.4]. A center frequency is defined & the propagation of a Gaussian beam at that frequency defines the optical axis. Small deviations around that central path caused by small frequency deviations will be described by the E and F terms. If F is made frequency dependent, then it will give rise to the angular dispersion upon refraction or diffraction.

To obtain the value of F, we use the grating equation given by [B.4]

$$\sin\theta_1 + \sin\theta_2 = \frac{2\pi cn}{\omega d} \tag{D.40}$$

Where c is the speed of light, n is the medium in which the grating is immersed, ω is the center frequency of the beam & d is the groove spacing of the grating.

From equation, F is obtained to be [B.4]

$$F_0 = \frac{2\pi cn^2}{\omega^2 d\cos\theta_2}\Delta\omega \tag{D.41}$$

Where F_0 is the first-order term & $\Delta\omega$ is the frequency shift from the center frequency.

The diffraction grating matrix for angular frequency dispersion in the first order is given by

$$\begin{bmatrix} x_2 \\ x_2' \\ 1 \end{bmatrix} = \begin{bmatrix} \frac{\cos\theta_2}{\cos\theta_1} & 0 & 0 \\ 0 & \frac{\cos\theta_1}{\cos\theta_2} & \frac{2\pi cn^2}{\omega^2 d\cos\theta_2}\Delta\omega \\ 0 & 0 & 1 \end{bmatrix} \begin{bmatrix} x_1 \\ x_1' \\ 1 \end{bmatrix} \tag{D.42}$$

For higher order terms of dispersion, we use the following definitions

$$A = \frac{\cos\theta_2}{\cos\theta_1}\left(1 - \frac{1}{n}\sin\theta_2 F_0\right) \tag{D.43}$$

$$D = \frac{\cos\theta_1}{\cos\theta_2}\left(1 - \frac{1}{n}\tan\theta_2 F_0\right) \tag{D.44}$$

$$F = F_0\left[1 - 2\frac{\Delta\omega}{\omega} + \frac{1}{2}\tan\theta_2 F_0\right] \tag{D.45}$$

B.4 Plot of the diffraction grating ray matrix

We will plot the grating equation $\theta_2 = \sin^{-1}\left(\frac{\lambda_0}{d} - \sin(\theta_1)\right)$ and use the grating ray matrix to compare the values with a specific region of the input angle.

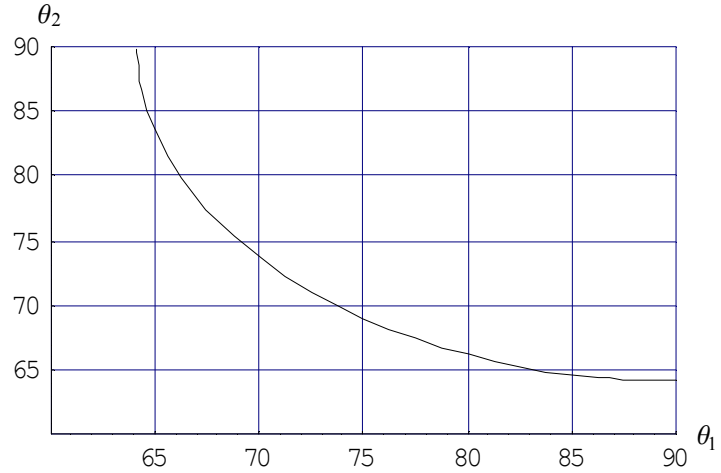

Figure B.3: Plot of grating equation, input angle vs. output angle for the following parameters: λ_0 =950nm,d=500nm, θ_1 from 60 deg to 90 deg.

Assuming no angular frequency dispersion, we use the 2X2 ABCD matrix & substituting the values λ_0 =950nm, d=500nm, θ_1 =75 deg, matrix equation will be given by

$$\begin{bmatrix} x_2 \\ x_2' \end{bmatrix} = \begin{bmatrix} 1.37965 & 0 \\ 0 & 0.724823 \end{bmatrix} \begin{bmatrix} x_1 \\ x_1' \end{bmatrix} \tag{D.46}$$

To observe the change in output angle with the change in input angle, we use the equation

$$x_2' = 0.724823 x_1' \tag{D.47}$$

We vary $x_1^{'}$ from -5 deg to +5 deg to get a total change of 70 deg to 80 deg in the input angle. i.e. $(\theta_2 - x_2^{'})$ is plotted with respect to $(\theta_1 + x_1^{'})$

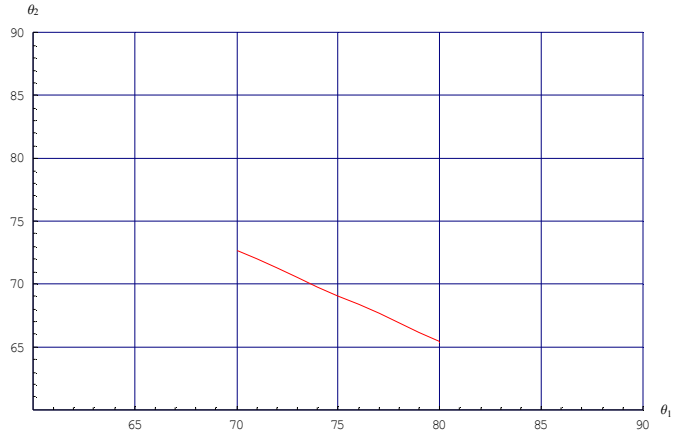

Figure B.4: The plot of the matrix for λ_0 =950nm,d=500nm, for a slope variation of -5 deg to +5 deg from the initial angle of θ_1 =75 deg

The superimposed images are shown below.

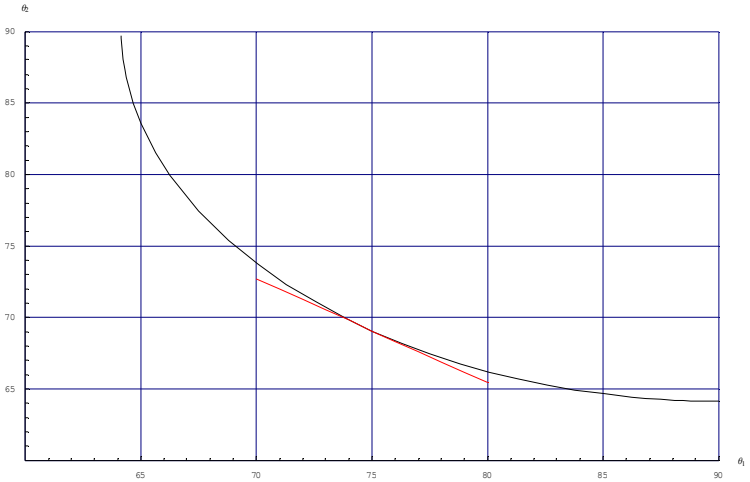

Figure B.5: The red line indicates the linearised values of the output angle from the ray matrix for λ_0 =950nm,d=500nm, for a tilt of -5 deg to +5 deg from the initial angle of θ_1 =75 deg

REFERENCES

2.1 Davis, Christopher C. Lasers and Electro-Optics: Fundamentals and Engineering. Cambridge [England]: Cambridge University Press, 1996

2.2 Singh, Jasprit Semiconductor Optoelectronics: Physics and Technology. McGraw-Hill series in electrical and computer engineering. New York: McGraw-Hill, 1995.

2.3 Thompson, G. H. B. Physics of Semiconductor Laser Devices. Chichester [Eng.]: J. Wiley, 1980.

2.4. Kapany, Satinder Optical Waveguides, Boston: Academic Press Inc., 1972.

2.5. Paschotta, Rüdiger "Encyclopedia of Laser Physics and Technology" [Online document], [2007 May 20], Available at HTTP: http://www.rp-photonics.com/encyclopedia.html

2.6. Broad Area Diode Lasers, Multi Mode Available at HTTP: http://195.145.23.110/BA_Info.php Copyright 1993-2007 Sacher Lasertechnik Group. All rights reserved.

2.7. Fukuda, Mitsuo Reliability and Degradation of Semiconductor Lasers and LEDs. Boston: Artech House, 1991.

3.1 Stelmakh, Nikolai Measurement of Spatial Modes of Broad-Area Diode Lasers With 1-GHz Resolution Grating Spectrometer, IEEE PHOTONICS TECHNOLOGY LETTERS, VOL. 18, NO. 15, Pages: 1618-1820, Aug, 2006

3.2 Dr. Nikolai Stelmakh (private communications)

4.1 Gerrard, Anthony & Burch, James M. Introduction to Matrix Methods in Optics. Wiley series in pure & applied optics. London: Wiley, 1975.

4.2 Siegman, A. E. Lasers. Mill Valley, Calif: University Science Books, 1986.

A.1 Halbach, Klaus Matrix Representation of Gaussian Optics, Am. J. Phys. 32, 90, 1964

B.1 Siegman, A. E. ABCD-matrix elements for a curved diffraction grating , J. Opt. Soc. Am. A, Vol. 2, No. 10, 1793, Oct 1985

B.2 Siegman, A. E. Lasers. Mill Valley, Calif: University Science Books, 1986.

B.3 Kanstad, S. O. and Wang, G. Laser resonators folded by diffraction gratings, Appl. Opt. Vol. 17, No. 1, 87-90, Jan 1978

B.4 Martinez, O.E. Matrix Formalism for Pulse Compressors Quantum Electronics, IEEE Journal of, Vol.24, No.12, 2530-2536, Dec 1988

BIOGRAPHICAL INFORMATION

Sheldon Fernandes received his Bachelors of Engineering in Electronics & Communications from MIT, Manipal, India. He worked for a software company in India for 2 years. He is pursuing his MS degree in Electrical Engineering from UT, Arlington. He has worked at the High Power Laser Diode Lab at UT, Arlington. His research interests include integrated optics, optical systems, I.C fabrication & VLSI.